



RESEARCH ARTICLE

10.1029/2023JD039251

Key Points:

- Aerosols enhance charge separation and lightning discharges due to a greater ice-crystal concentration and larger graupel size
- Aerosols lead to inverted charge structure with strong positive-charge region, producing high percentage of positive cloud-to-ground strokes
- Graupel particles gain positive charge at upper levels in the presence of higher supercooled cloud water under polluted conditions

Correspondence to:

Z. Li,
zhanqing@umd.edu

Citation:

Sun, M., Li, Z., Wang, T., Mansell, E. R., Qie, X., Shan, S., et al. (2024). Understanding the effects of aerosols on electrification and lightning polarity in an idealized supercell thunderstorm via model emulation. *Journal of Geophysical Research: Atmospheres*, 129, e2023JD039251. <https://doi.org/10.1029/2023JD039251>

Received 15 MAY 2023

Accepted 23 NOV 2023

Author Contributions:

Conceptualization: Mengyu Sun, Zhanqing Li

Formal analysis: Mengyu Sun

Funding acquisition: Zhanqing Li, Tao Wang







Methodology: Mengyu Sun, Edward R. Mansell

Supervision: Zhanqing Li, Tao Wang

Writing – original draft: Mengyu Sun

Writing – review & editing: Edward R. Mansell, Xiushu Qie, Maureen Cribb

Understanding the Effects of Aerosols on Electrification and Lightning Polarity in an Idealized Supercell Thunderstorm via Model Emulation

Mengyu Sun^{1,2} , Zhanqing Li³ , Tao Wang¹, Edward R. Mansell⁴ , Xiushu Qie⁵ , Siyu Shan³ , Dongxia Liu⁵ , and Maureen Cribb³

¹Department of Civil and Environmental Engineering, The Hong Kong Polytechnic University, Hong Kong, China, ²Faculty of Geographical Science, Beijing Normal University, Beijing, China, ³Department of Atmospheric and Oceanic Science, University of Maryland, College Park, MD, USA, ⁴NOAA/National Severe Storms Laboratory, Norman, OK, USA, ⁵Key Laboratory of Middle Atmosphere and Global Environment Observation, Institute of Atmospheric Physics, Chinese Academy of Sciences, Beijing, China

Abstract Aerosol effects on the lightning intensity and polarity of a continental supercell storm were investigated using a three-dimensional lightning scheme within the Weather Research and Forecasting model. We find that both intra-cloud (IC) and cloud-to-ground (CG) flashes are enhanced by the increasing number of cloud condensation nuclei (CCN), especially the percentage of positive CG (+CG) strokes peaking at 42%. Electrical characteristics of the storm varied in different aerosol scenarios through microphysical processes. Added aerosols increase the number of cloud droplets and ice-phase hydrometeors. The greater ice-crystal concentration and larger graupel size ensure sufficient charge separation, leading to higher charge density and more lightning discharges. In addition, an inverted polarity charge structure with a strong positive-charge region in the mid-levels was formed mainly due to the positively charged graupel in the presence of higher supercooled cloud water content. Positive lightning channels originating from this positive-charge region propagated to the ground, producing more +CG strokes. When the aerosol concentration was low, the charge density in the upper positive-charge region was much lower due to smaller ice-particle content. Consequently, there were barely any +CG strokes. Most of the negative CG flashes deposited positive charge in the lower negative-charge region.

Plain Language Summary The possible effects of aerosols on lightning intensity and polarity were investigated using an explicit lightning scheme within a weather forecast model. Added aerosols invigorated intra-cloud flashes and cloud-to-ground (CG) flashes in continental convection. A noticeably high fraction of positive CG lightning was also identified under polluted conditions. Elevated cloud condensation nuclei concentration increased the ice particle content and graupel size, leading to enhanced charge separation and lightning activity. An inverted-polarity charge structure appeared owing to the positively charged graupel in the presence of greater supercooled cloud water amounts. This charge distribution was manifested in the lightning activity, showing that positive channels propagated to the ground, generating more positive CG strokes under polluted conditions.

1. Introduction

Lightning activity can be invigorated with elevated aerosol emissions (Feudale & Manzato, 2014; Hu et al., 2019; Li et al., 2016, 2019; Orville et al., 2001; K. Qie et al., 2021; Thornton et al., 2017; Westcott, 1995), while convection and lightning might be inhibited by too many aerosols (Altaratz et al., 2010; Q. Wang et al., 2018; P. Zhao et al., 2020). More aerosols increase the cloud droplet number and the latent heat release (Lynn et al., 2007; Rosenfeld et al., 2008). More cloud droplets can thus be lifted above the freezing level, leading to higher supercooled liquid water content and more ice-phase particles (Fan et al., 2017), ultimately affecting charge separation and lightning activity (Mansell & Ziegler, 2013; Sun, Qie, et al., 2023; Takahashi, 1978). Bell et al. (2009) reported a weekly cycle in precipitation and lightning in the southeastern US, associated with added aerosols due to urban pollution in the midweek compared to the weekend. This may be considered an indicative for an indirect effect of aerosols on the microphysics of thunderstorms. Stallins et al. (2013) and Coquillat et al. (2013) also reported similar results for the Atlanta region, US and Paris, France, respectively. In China, not only distinct weekly cycles were found, but also the phases of the cycle are opposite in the central and eastern regions dominated by strongly and weekly absorbing aerosols whose effects on convection are at odds with each other (Yang et al., 2016).

© 2023. The Authors.

This is an open access article under the terms of the [Creative Commons Attribution License](https://creativecommons.org/licenses/by/4.0/), which permits use, distribution and reproduction in any medium, provided the original work is properly cited.

Aerosols can also influence the percentage of intra-cloud (IC) and cloud-to-ground (CG) flashes, as well as the percentage of positive/negative CG lightning (Guo et al., 2016; Murray et al., 2000). Positive CG (+CG) flashes can be correlated with storm severity and even tornado occurrence, although they only account for a small fraction of the total flashes that most storms produce (Carey et al., 2003; Schultz et al., 2011; Yuan et al., 2020). During the 2019–2020 Australian wildfire, Liu et al. (2021) found that added aerosols invigorate both negative CG (−CG) and positive intra-cloud (+IC) lightning in moist oceanic convection. However, Lyons et al. (1998) reported that thunderstorms generate a high fraction of lightning with positive polarity (+CG) during a pollution episode under exceptionally dry conditions over the central US. Fernandes et al. (2006) found an enhancement of +CG strokes in smoke-invigorated clouds in Brazil. A tripole charge configuration with a lower positive-charge center and no +CG flashes was observed by X. Qie et al. (2005) in a thunderstorm over the Tibetan Plateau. An inverted dipole with an additional negative-charge region below the main positive-charge center was proposed to explain the enhancement of +CG flashes in dust-ingested clouds over the Mediterranean Sea (Yair et al., 2021). The electrical processes under different aerosol conditions, especially the lightning polarity and its origins, vary in different studies.

Observing the details of in-cloud processes (e.g., graupel, snow, and ice crystals) is challenging, especially in terms of any causal effect. However, numerical simulations can be used to study aerosol effects on storm-scale electrification and lightning discharges (e.g., Khain et al., 2010; Mitzeva et al., 2006). Mansell and Ziegler (2013) and Tan et al. (2017) employed three- and two-dimensional models, respectively, to investigate the response of storm-scale electrical processes to aerosol concentration. Additionally, P. Zhao et al. (2015) used the Weather Research and Forecasting (WRF) model to investigate thunderstorm electrification under clean and polluted conditions, finding that elevated aerosols increased the cloud water content (CWC) and ice-phase particle concentration. More studies have been devoted to investigating the relationship between aerosols and lightning production. For instance, Shi et al. (2015) related the lightning flash rate to the ice-phase particle mass in thunderclouds, finding that an increase in aerosol concentration led to increases in charge separation and lightning flash rate. To compare the differences between the microphysics and electrification of polluted and pristine thunderclouds, Y. Wang et al. (2011) used the lightning potential index to represent lightning activity, which is linked to updrafts, ice-phase particles, and liquid water contents from WRF model simulations. A bulk lightning model was used by Sun et al. (2021) (hereafter referred to as Sun21) to estimate the flash origin density by reducing and redistributing charges throughout a cylindrical region after each discharge (Fierro et al., 2013). These simulations were mainly based on a simple empirical formula or bulk lightning parameterization. To investigate in detail the effects of aerosols on lightning intensity and polarity in thunderclouds, this study presents simulation results obtained using a model with explicit treatments of three-dimensional discharge processes.

2. Model Description and Experiment Design

We used the electrified WRF model version 4.3.1 (WRF-ELEC; Fierro et al., 2013) coupled with a sophisticated three-dimensional lightning scheme (MacGorman et al., 2001; hereafter M01). The model includes a double-moment microphysics scheme and an explicit charging parameterization (Mansell et al., 2005).

The National Severe Storms Laboratory bulk microphysics scheme (Mansell et al., 2010) assumes gamma size distribution and predicts both mass and number concentrations for six hydrometeor species (cloud droplets, raindrops, graupel, snow, hail, and ice crystals). Mansell et al. (2010) provide further descriptions of the scheme. Only details relevant to this work are presented here. The cloud nucleation is predicted following Twomey (1959). The activated aerosols are represented by cloud condensation nuclei (CCN), and their bulk concentration is prescribed by Equation 1:

$$N_{\text{CCN}} = \text{CCNC} \times S^k, \quad (1)$$

where CCNC is the assumed CCN concentration, S is the supersaturation, and $k = 0.6$ is the exponent in Twomey (1959) CCN relationship. The number of un-activated CCN is tracked, with the model depleting local CCN either in the cloud or at the cloud base when droplets are activated (Mansell & Ziegler, 2013). Droplet condensation growth is treated explicitly (i.e., no saturation adjustment), which can leave residual supersaturation. Cloud droplet nucleation, deposition, evaporation, condensation, ice multiplication, freezing and melting, riming, sublimation, cloud ice nucleation and aggregation, and conversions between hydrometeor species are all included in the microphysical processes. High-density frozen drops (e.g., small hail) fall in the graupel

category because graupel particle density can be predicted within the allowed range (300–900 kg m⁻³). Collected low-density snow and ice crystals are assumed to add to the graupel volume at the minimum density allowed for graupel (Mansell et al., 2010).

Electrification parameterizations (Mansell et al., 2005) consist of non-inductive charge separation, which is independent of the ambient electric field transfer charge between graupel and small ice and snow particles. The non-inductive charging is based on the riming accretion rate (RAR; Saunders & Peck, 1998). The mean separated charge (δq) is calculated for rebounding collisions between graupel-hail and snow-cloud ice (Fierro et al., 2013), using the non-inductive critical charging curve as a function of temperature and RAR:

$$\delta q = BD_{n,I}^a \left(\overline{V}_g - \overline{V}_I \right)^b q_{\pm}(\text{RAR}), \quad (2)$$

where B , a , and b are subjected to crystal size; $D_{n,I}$ is the diameter for the cloud ice (or snow) category; \overline{V}_g and \overline{V}_I are the mass-weighted mean terminal fall speeds for graupel and cloud ice (or snow), respectively; and $q_{\pm}(\text{RAR})$ is the charge separation as a function of RAR. The critical RAR curve defines the positive and negative graupel charging zones, which is a piece-wise continuous function given by Mansell et al. (2005):

$$\text{RAR}_{\text{crit}} = \begin{cases} s(T) : T \geq -23.7^{\circ}\text{C} \\ k(T) : -23.7^{\circ}\text{C} > T > -40^{\circ}\text{C}, \\ 0 : T \leq -40^{\circ}\text{C} \end{cases} \quad (3)$$

where $s(T)$ is the polynomial fit as a function of temperature T :

$$\begin{aligned} s(T) = & 1.0 + 7.9262 \times 10^{-2}T + 4.4847 \times 10^{-2}T^2 \\ & + 7.4754 \times 10^{-3}T^3 + 5.4686 \times 10^{-4}T^4 \\ & + 1.6737 \times 10^{-5}T^5 + 1.7613 \times 10^{-7}T^6, \end{aligned} \quad (4)$$

and

$$k(T) = 3.4 \left[1.0 - \left(\frac{|T + 23.7|}{-23.7 + 40.0} \right)^3 \right]. \quad (5)$$

Inductive charge separation (i.e., electric field-dependent) in rebounding graupel-droplet is also considered. Following a set of tests, Mansell et al. (2010) found that the rate of inductive charging is much weaker than noninductive charge separation, but it is important for the formation of lower-charge regions. The electric field potential is solved using the “black box multigrid” elliptic equation solver (Dendy & Moulton, 2010).

The lightning model used in this study differs from that used by Fierro et al. (2013). We use an explicit three-dimensional scheme (M01) for discrete lightning discharges. This scheme considers the discharge process as individual flashes (i.e., IC and CG flashes) rather than a bulk process across the domain of simulation (i.e., Ziegler & MacGorman, 1994, hereafter ZM94; Fierro et al., 2013). Currently, the M01 scheme is less practical for real-time use because it is more time consuming than the ZM94 scheme (about 3 times more) for comparable flash density. Breakdown is initiated when the electric fields exceed a height-dependent threshold E_{init} provided by Dwyer (2003). After that, the starting point is selected randomly among grid points with $|E| > E_{\text{init}} - \delta E_{\text{init}}$, where $\delta E_{\text{init}} = 10 \text{ kV m}^{-1}$. The M01 scheme propagates an explicit channel parallel and antiparallel in a time step from the point of initiation. The lightning channel at each end initially stops at points where the ambient magnitude falls below a fixed threshold [set to 90% of E_{init} , as in Fierro et al. (2015)]. A channel end is terminated if it reaches the ground. Others are allowed to extend to all contiguous points having $|\rho| > |\rho_{\text{chan}}|$ and $|\phi| > |\phi_{\text{end}}|$, where ρ is the net charge density at a grid point, ρ_{chan} is the minimum value of charge density for a point to be involved in channels, and ϕ and ϕ_{end} represent the ambient electrical potential at a grid point and at the channel end before development, respectively. All grid points satisfying these criteria can become involved in discharging processes. The proportion of the available charge density neutralized by individual flashes is set to 30% [as in M01]. The lightning model computes flash rates, the flash extent density (FED), and lightning channel counts

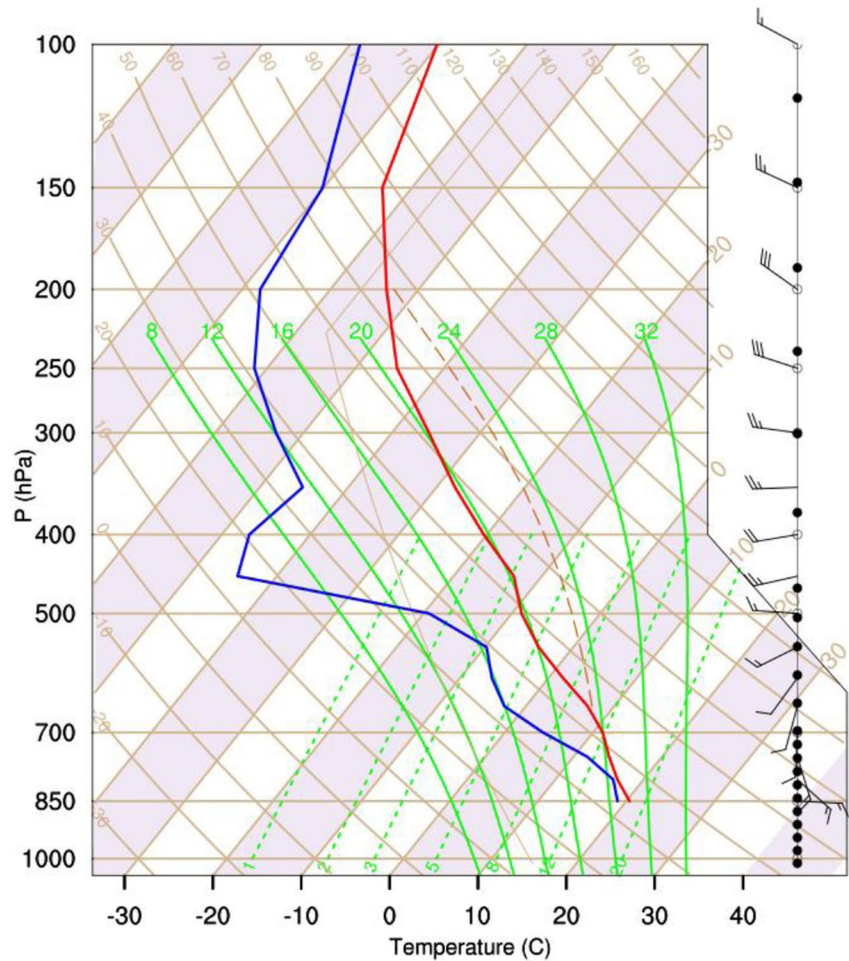


Figure 1. The sounding used to depict initial conditions for the simulations.

(LCCs) of total lightning activity (IC and CG strokes). In the present study, the FED is the total number of flashes developing into the grid column. The LCC represents the integration of all positive or negative channel counts at a given altitude in each column every time step.

To investigate in detail the effect of aerosols on lightning discharges in thunderclouds, an outbreak supercell thunderstorm with a large amount of convective available potential energy was chosen and simulated. This storm occurred in western Texas on 2 June 1995, significantly intensifying on the immediate cool side of the outflow boundaries (Gilmore & Wicker, 2002; hereafter GW02). The present study therefore only included supercells on the cool side. Figure 1 shows the thermodynamic profile used for simulations, taken from Fierro et al. (2006). Gilmore (2000) provides details of this storm. The purpose for choosing this profile is to provide a suitable thunderstorm environment so that the aerosol effects on electrification and lightning polarity can be investigated.

Simulations were performed in a 400-km \times 400-km domain, with a constant grid spacing of 1 km in the horizontal. The vertical grid had 61 vertical levels, with the top set to 20 km. Each simulation was run for 240 min, with a 5-s time step. Although the storm did not dissipate after 240-min simulation, the lightning flash rate and +CG flashes did increase in the polluted run, which is sufficient for our analysis. Convection was initiated by a thermal bubble having a perturbation of +2.5 K. The dominant CG polarity of the storms observed on 2 June 1995 depends on the local environment (GW02). Therefore, we designed all sensitivity experiments using a horizontally homogeneous environment in this study instead of a heterogeneous one (Fierro et al., 2006), with the purpose of examining aerosol impacts on lightning polarity. Besides the continental case [$900 \times (\rho_{\text{air}}/\rho_0) \text{ cm}^{-3}$, where $\rho_0 = 1.225 \text{ kg m}^{-3}$, and ρ_{air} is air density, hereafter Ctrl run], additional simulations were designed based on the Ctrl run by changing CCN concentrations to $350 \times (\rho_{\text{air}}/\rho_0) \text{ cm}^{-3}$ (i.e., clean run) and $1,400 \times (\rho_{\text{air}}/\rho_0)$

cm^{-3} (i.e., polluted run) in the initial conditions. There were no observations of IC lightning from the National Lightning Detection Network for this case (Fierro et al., 2006). The variation of CG lightning flashes observed in actual storms was only reproduced in the Ctrl run. Simulated flashes were dominated by negative polarity, consistent with the lightning behaviors before crossing the boundaries. The convective characteristics (e.g., 40-dBZ echo-top height) of the simulated storms in the Ctrl case were also similar to observations (GW02). For comparison, the CCN concentration in the clean run was selected according to simulation tests conducted by Mansell et al. (2010). This concentration can promote large cloud droplet diameters to sustain an effective collision-coalescence process. The initial number concentration for the polluted case was set following Mansell et al. (2005), which was higher than the number concentration in the Ctrl run. The high prescribed CCN concentration guaranteed small droplets that could efficiently hinder the warm-rain process in the model (Dye et al., 1974; Mansell et al., 2005).

3. Results

3.1. Aerosol Effects on Convection and Microphysics

To investigate whether increasing the CCN concentration changes convection, Figure 2 shows the spatial distribution of radar reflectivity during different stages of the storm for different aerosol scenarios. Based on the characteristics of reflectivity and lightning activity (van den Broeke et al., 2008; Liu et al., 2021; Lu et al., 2022; C. Zhao et al., 2022), the different stages of storm development, that is, initial (Figures 2a, 2d, and 2g), developing (Figures 2b, 2e, and 2h), and pre-mature (Figures 2c, 2f, and 2i), were identified. Convection developed later in the polluted run than in the Ctrl and clean cases. The morphologies of radar reflectivity during the different periods were similar, with a new convective cell developing toward the north under clean conditions (Figure 2c). Figure 2 also depicts FED at different times. The spatial distribution of simulated lightning was consistent with that of radar reflectivity at the different stages. Lightning was concentrated in areas where the radar echo was greater than 40 dBZ. FEDs were enhanced as the CCN concentration increased. We further examined convective intensities for the different runs by comparing profiles of radar reflectivity and vertical velocity (Figure 3). The maximum updraft speed above 10 km (Figure 3a) and the 55-dBZ echo volume (Figure 3b) were significantly increased in the polluted case, indicating much stronger convection.

The cloud water number and ice-phase volume (i.e., ice crystals) also increased under polluted conditions. Figures 4–6 show the time-height variations of microphysical properties for different hydrometeors. For each quantity, properties were averaged horizontally over the entire region at a given altitude. The added CCN concentration increased the number of droplets while decreasing their radii. The droplet number concentration peaked below 3 km in the clean case, with higher values up to ~8 km for the polluted case (Figures 4a and 4e). In the clean run, the largest cloud droplets (26.5 μm radius, Figure 7a) appeared around 9 km. Cloud droplets with maximum radius of 23.1 μm in the polluted run was smaller than in the clean case, appearing above 10 km. These smaller droplets suppressed the collection-coalescence process. The formation of more cloud droplets in the polluted run induced stronger convection, as previously discussed. As a result, more droplets lifted by stronger updrafts to higher levels increased the supercooled CWC and enhanced mixed-phase processes, leading to larger ice particle mixing ratios at upper levels ($< -40^\circ\text{C}$, roughly 8–14 km, Figures 5b, 5d, and 5f). Rime splintering (i.e., the Hallett-Mossop process) can contribute to larger ice crystal number concentrations within a certain temperature range and is sensitive to the droplet size distribution (Mansell & Ziegler, 2013). Homogeneous freezing of cloud droplets from 8 to 14 km primarily led to an increase in ice particle content (Straka & Mansell, 2005). Table 1 summarizes the domain-averaged microphysical characteristics of different hydrometeors. These values were averaged over the entire simulation period. The ice crystal content was much greater under polluted conditions, with domain averages of $272.2 \times 10^3 \text{ kg}^{-1}$ for the polluted run and $37.5 \times 10^3 \text{ kg}^{-1}$ for the clean run. The mean-mass radius of ice crystals in the polluted run (21.9 μm) was smaller than in the clean run (30.7 μm). The largest ice crystals in the polluted case appeared above 8.5 km, while in the clean case, they appeared around 8 km (Figure 7d).

Increasing the CCN concentration can effectively suppress the warm-rain processes (Figures 4d and 4f) due to the reduced conversion from smaller droplets to raindrops. Under polluted conditions, the rain water content was much less than that in the clean case. Compared to cloud droplets and ice crystals, graupel and snow particle contents were much less in the polluted case. Previous studies have reported that there could be more graupel in the mixed-phase region (e.g., Y. Wang et al., 2011; P. Zhao et al., 2015). However, other studies have found a decrease

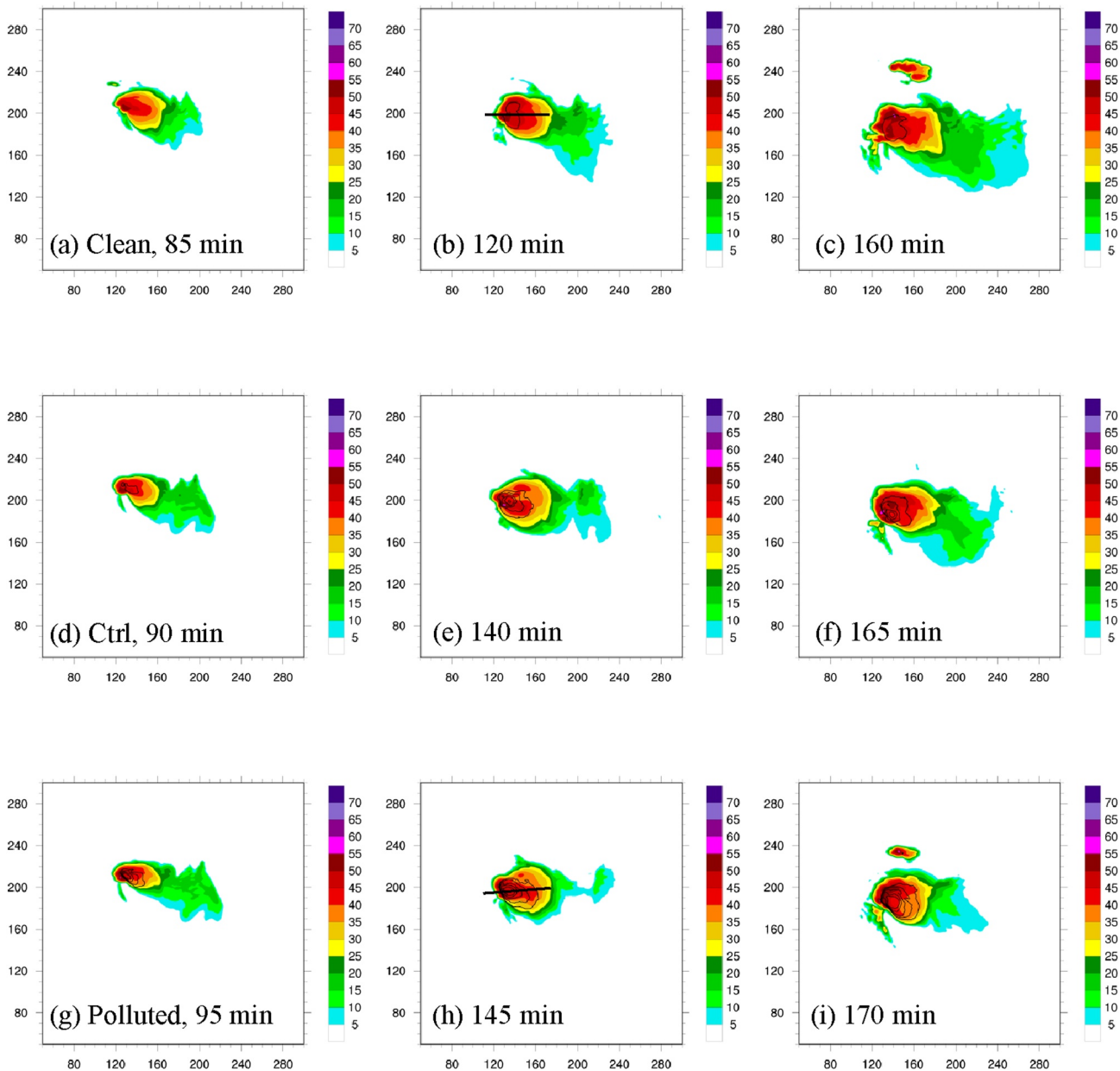


Figure 2. Series of simulated composite radar reflectivity (shaded, unit: dBZ) and the flash extent density (FED) (contours, unit: 5 min^{-1}). (a)–(c) Clean-case simulations at 85 min, 120 min, and 160 min (d)–(f) Ctrl simulations at 90 min, 140 min, and 165 min (g)–(i) Polluted-case simulations at 95 min, 145 min, and 170 min. FED contours start at $40 (5 \text{ min})^{-1}$, with intervals of $40 (5 \text{ min})^{-1}$. The thick black lines in (b) and (h) highlight the locations of the vertical cross sections in Figures 14 and 13, respectively.

in the graupel content (e.g., Tan et al., 2017; Sun21). A possible explanation is that the additional mass is kept in droplets that freeze into ice crystals, reducing the net precipitation efficiency. Reduced raindrop freezing leads to a reduction in the graupel mass mixing ratio. The snow content is also reduced because of its similar growth process to graupel in simulations: collection of droplets or cloud ice (Mansell et al., 2010; Zrnice et al., 1993). The mean-mass radius of graupel for the polluted case was larger than in the clean case (Figure 7 and Table 1), mainly resulting from the lower number concentration. The difference in snow particle size between polluted and clean cases was small (Figure 7e). This is mainly because the collected snow particles were assumed to add to the graupel volume, resulting in a further decrease in snow content after 120 min (Figures 6a, 6c, and 6e). Small hail can be represented by frozen drops in the graupel category (Mansell et al., 2010). The change in hail content here was thus not significant with increasing CCN concentration. Figure 7f displays domain-averaged mean-mass

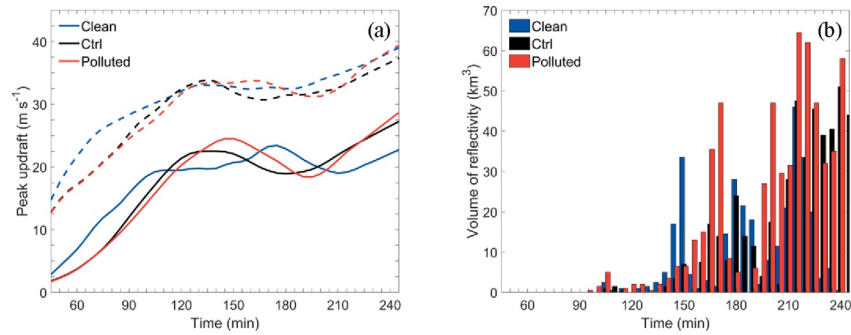


Figure 3. Time evolution of (a) maximum updraft speed (m s^{-1}) at all altitudes (dashed lines) and above 10 km (solid lines), and (b) volume of radar reflectivity (km^{-3}) greater than 55 dBZ for different cases. The blue, black, and red curves and bars represent clean, Ctrl, and polluted cases, respectively.

radii of hail particles. With the reduced number concentration (Figures 6b, 6d, and 6f), hail sizes increased with the added CCN concentration.

3.2. Aerosol Effects on the Evolution of Electricity

The vertical cross-section of the total net charge illustrates the charge structure at different stages of the simulations under clean, Ctrl, and polluted conditions (Figure 8). A charge configuration with negative charge below positive charge (i.e., a normal dipole) was seen in the clean run. Compared to the clean case, a significant inverted dipole (i.e., negative charge with positive charge below it) was simulated in the Ctrl and polluted runs. This inverted polarity charge distribution sustained a negative-charge region that later appeared beneath the main positive-charge region in the polluted case (Figure 8h). The charge density of the polluted run was greater than that of the clean run, with a maximum positive-charge density of more than $+0.5 \text{ nC m}^{-3}$ (Figure 8i). The peak charge density was about $+0.1 \text{ nC m}^{-3}$ in the clean run (Figure 8c).

To investigate the effect of aerosols on general electrical processes, Figure 9 shows the time evolution of the averaged non-inductive charging rate. Inductive charge separation was also considered, but its magnitude was around an order of magnitude lower than non-inductive charging so is not presented here. Figure 10 shows the time-height variation of the peak values of positive and negative charge density carried by graupel and cloud ice. According to Saunders and Peck (1998), graupel particles gain positive charges from rebounding collisions in the presence of a higher supercooled liquid water content in the 9–13 km layer ($<-40^\circ\text{C}$, Figure 9c). Under higher CCN conditions, graupel particles were charged positively within regions of higher CWC (8–10 km, Figures 9b and 9c), and the reverse for cloud ice. The peak values of positive charge density were much higher than the negative charge density carried by graupel in the polluted case (Figure 10c). Therefore, an inverted dipole appeared in the Ctrl and polluted cases, with a main positive-charge region located in the middle levels (Figures 8d and 8g). Under clean conditions, graupel was charged negatively with lower supercooled CWC at $\sim 10 \text{ km}$ ($<-40^\circ\text{C}$, Figures 9a and 10a), while cloud ice mainly gained positive charges (Figure 10b). These graupel particles and ice crystals corresponded to the lower negative-charge center and upper positive-charge center in the normal dipole, respectively (Figures 8a–8c). The non-inductive charging rates were clearly enhanced as the CCN concentration increased. By contrast, the charging rate was lower under clean conditions, resulting in lower values of charge density at upper altitudes (9–13 km, Figures 8a–8c). As Figure 9 shows, the averaged non-inductive charging rate was $\sim 0.3 \text{ pC m}^{-3} \text{ s}^{-1}$ for the Ctrl run, about half that of the polluted run. Under polluted conditions, the large ice particle content from 9 to 13 km played an important role in non-inductive electrification. Higher charging rates due to the much larger ice-phase particle content further led to an increase in charge density in the polluted case. Table 2 summarizes the averaged and maximum positive (and negative) charge density of different ice-phase particles. The averaged and maximum charge densities are the average and peak values over the entire simulated domain. The charge density carried by ice crystals and graupel in the polluted case is much larger than in the clean case (Figure 10 and Table 2). Lightning discharges only occur if the charge density is high enough for maximum electric field magnitudes to exceed the breakdown value. This suggests that elevated CCN concentrations may have enhanced the lightning frequency in this storm. Because the charge separation during rebounding collisions is considered between graupel-hail and cloud ice-snow, the polarity of charge carried by hail (and snow) particles

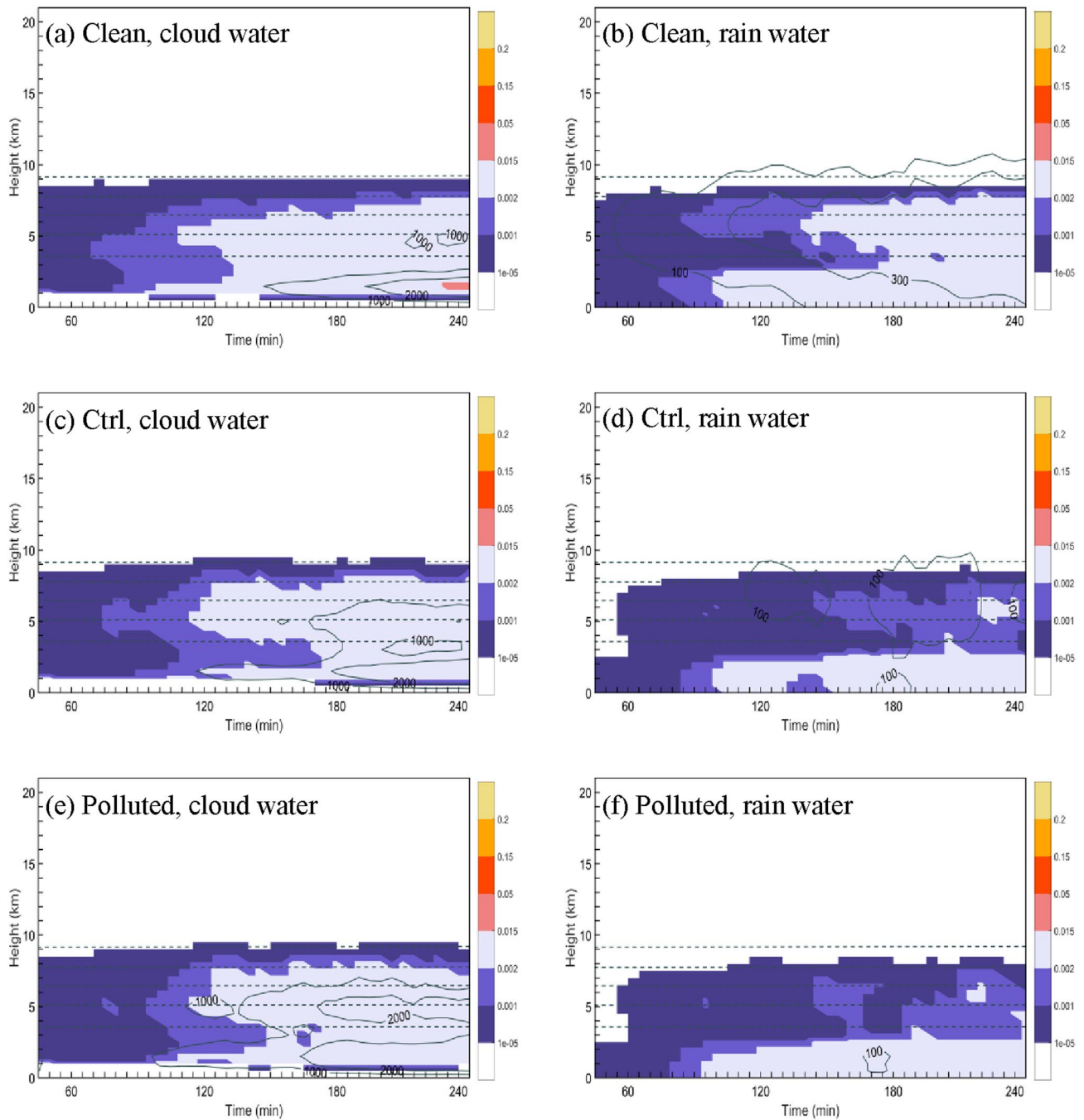


Figure 4. Time-height quantities: horizontally averaged mass mixing ratio (g kg^{-1} , shaded) and number concentration (kg^{-1} , contours) of (a) cloud water and (b) rain water in the clean run, (c) cloud water and (d) rain water in the Ctrl run, and (e) cloud water and (f) rain water in the polluted run. Contours in (a)–(f) for the cloud droplet number concentration are $1,000 \times 10^3$ and $2,000 \times 10^3 \text{ kg}^{-1}$, and for raindrops are 100 and 300 kg^{-1} . Dashed lines in (a)–(f) show the 0°C , -10°C , -20°C , -30°C , and -40°C isotherms.

and graupel (and cloud ice, figure not shown) were similar. Note that the charge density carried by hail in the clean case was close to zero (Table 2), mainly due to the smaller hail size and corresponding weaker electrification.

Concerning temporal variations, total flashes, including both IC and CG lightning, increased significantly after $t = 120$ min, peaking at ~ 220 min under polluted conditions (Figure 11). The number of total flashes was less in the clean and Ctrl cases. Note that the number and fraction of +CG flashes were increased in the polluted case, peaking at 165 min (19 strokes and 42%, respectively; Figure 11c). As Figure 11 shows, the value of +CG

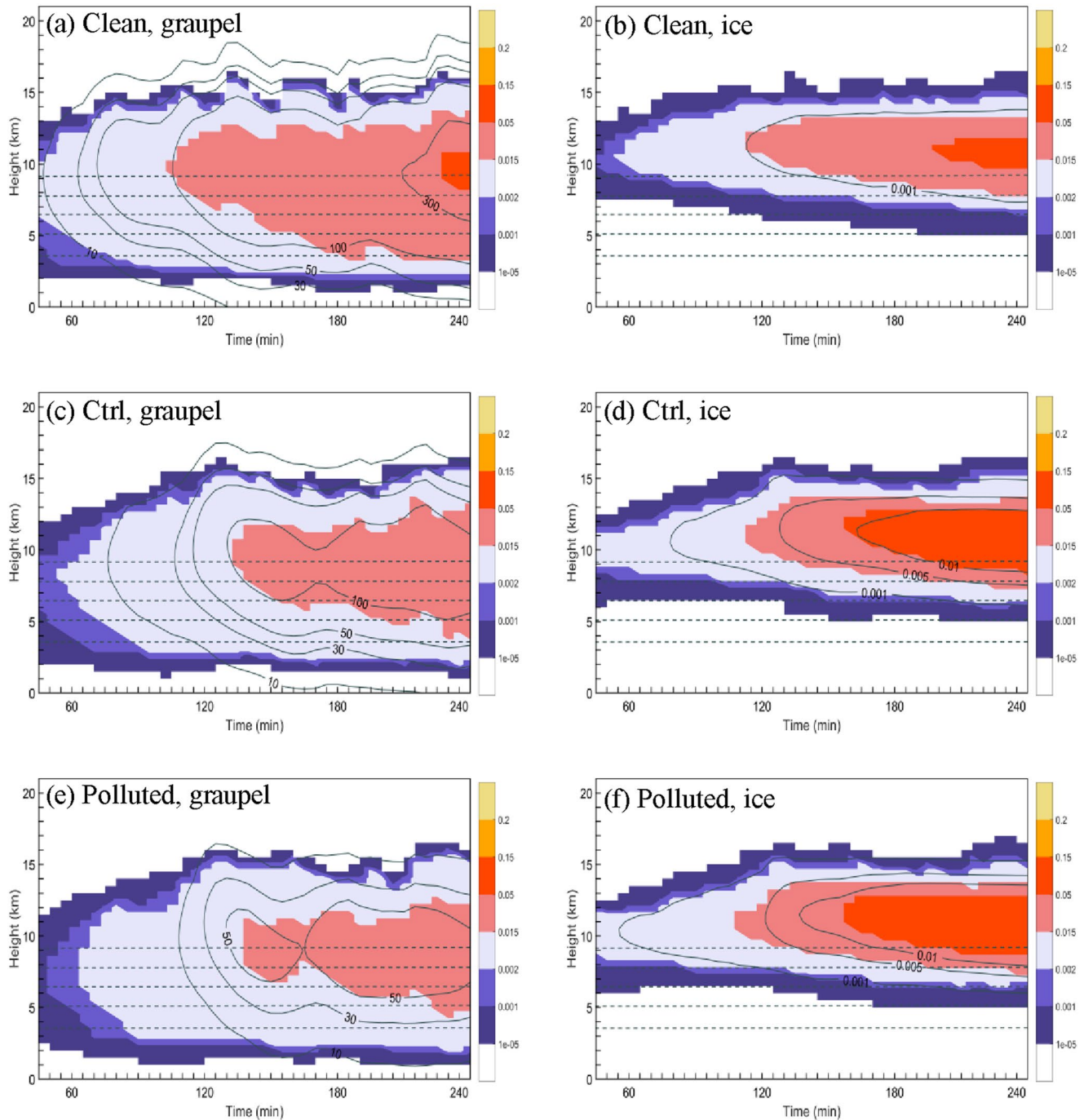


Figure 5. Time-height quantities for ice-phase particles: horizontally averaged mass mixing ratio (g kg^{-1} , shaded) and number concentration (kg^{-1} , contours) of (a) graupel and (b) ice in the clean run, (c) graupel and (d) ice in the Ctrl run, and (e) graupel and (f) ice in the polluted run. Contours for graupel are 10, 50, 100, 500, and 1,000 kg^{-1} , and for ice are 0.001×10^8 , 0.005×10^8 , and $0.1 \times 10^8 \text{ kg}^{-1}$. Dashed lines in (a)–(f) show the 0°C , -10°C , -20°C , -30°C , and -40°C isotherms.

strokes reached 62 flashes in the polluted run, while only 10 and 0 +CG flashes were initiated in the Ctrl and clean runs, respectively. To understand the effect of aerosols on the increase in +CG strokes, we further analyzed time-height variations of positively (and negatively) charged LCCs for different scenarios (Figure 12). Consistent with previous studies (e.g., Fierro et al., 2015; Kuhlman et al., 2006), the evolution of positive and negative LCCs coincided well in time with the maximum vertical velocity (Figure 3a) and the number concentration of ice-phase particles (Figure 5). The peak in LCCs at $t = 220$ min was associated with the peak in total flash (IC and CG) rate

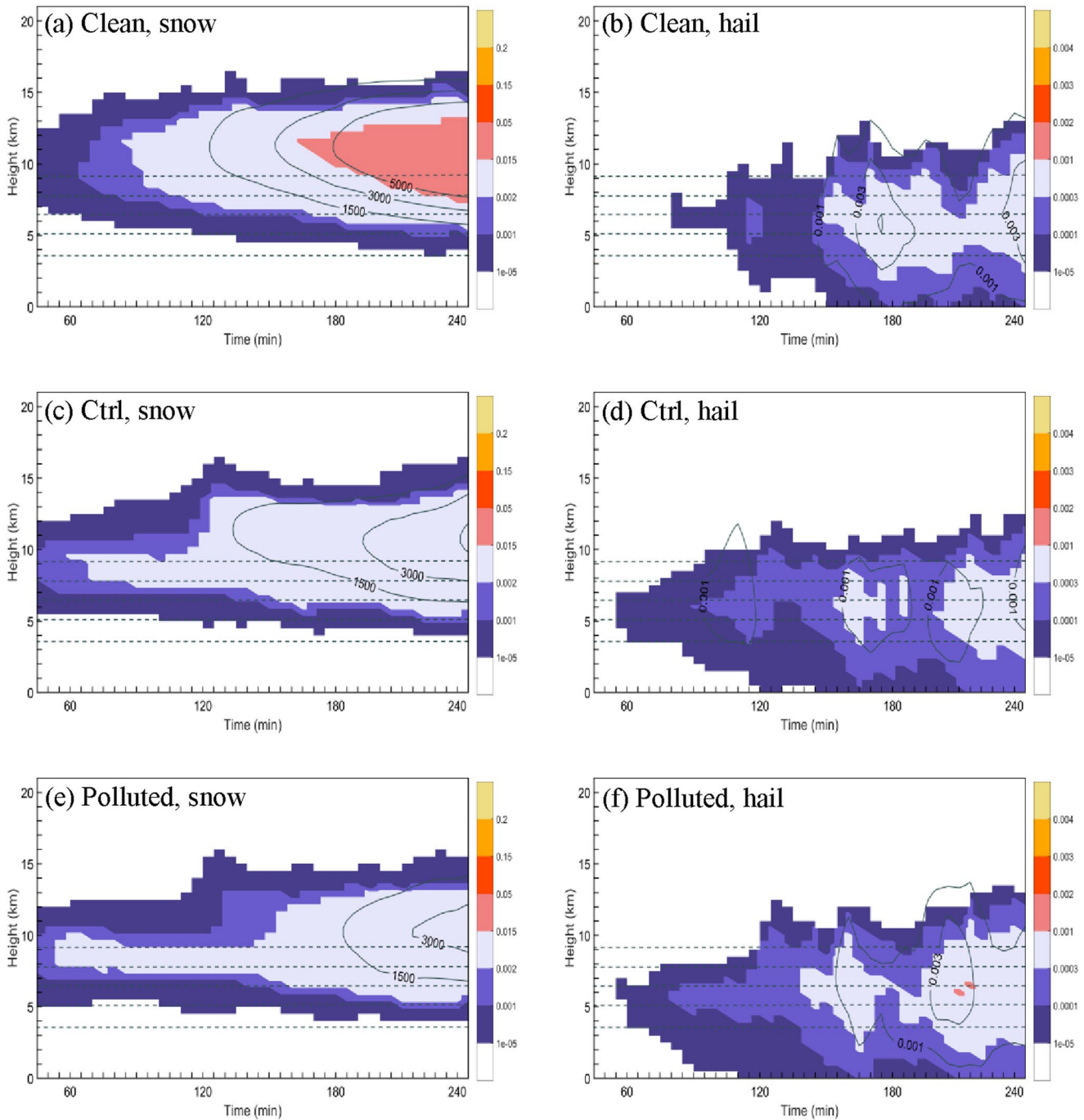


Figure 6. Time-height quantities for ice-phase particles: horizontally averaged mass mixing ratio (g kg^{-1} , shaded) and number concentration (kg^{-1} , contours) of (a) snow and (b) hail in the clean run, (c) snow and (d) hail in the Ctrl run, and (e) snow and (f) hail in the polluted run. Contours for snow are 1,500, 3,000, and 5,000 kg^{-1} , and for hail are 0.001 and 0.003 kg^{-1} . Dashed lines in (a)–(f) show the 0°C, -10°C, -20°C, -30°C, and -40°C isotherms.

under polluted conditions (Figures 11c and 12c). Positive LCCs reaching the ground at $t = 145$ min, 165 min, and 220 min were collocated with occurrences in +CG lightning.

The heights of charged LCCs correlated well with the heights of charge layers, with positive LCCs generally located at higher levels than negative LCCs, especially in the Ctrl and polluted runs (Figures 12b and 12c). These correlations are related to the peak in electric potential, which is accompanied by lightning discharge processes (e.g., M01; Mansell et al., 2010). The vertical distribution of the polarities of LCCs chiefly arose

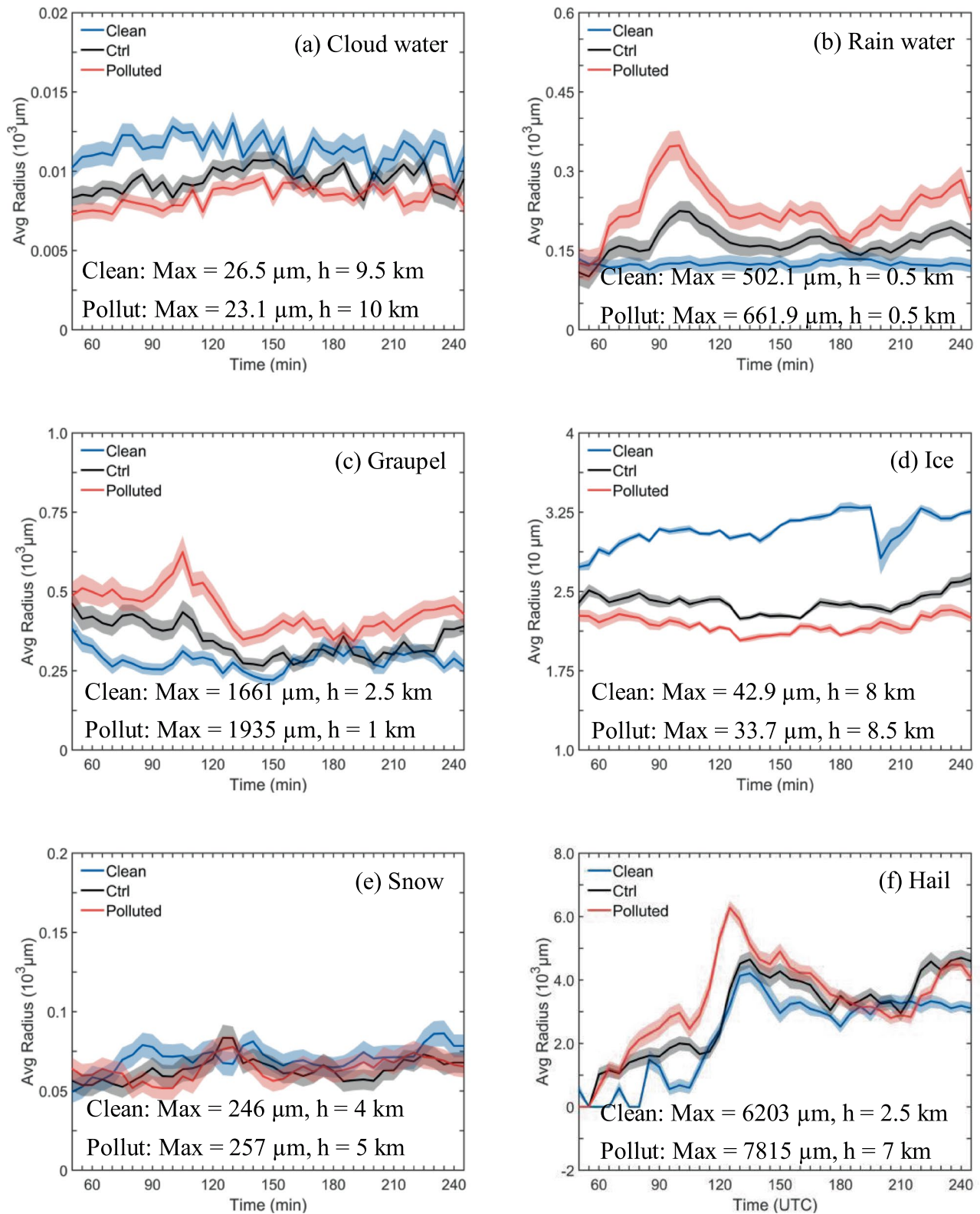


Figure 7. Temporal variations of domain-averaged mean-mass radii of different species: (a) cloud water, (b) rain, (c) graupel, (d) cloud ice, (e) snow, and (f) hail. The blue, black, and red lines represent the clean, Ctrl, and polluted cases. Shaded areas show the standard error of each parameter.

Table 1
The Domain-Averaged Characteristics of Hydrometeors

	Number concentration (10^3 kg^{-1})		Mean-mass radius (μm)	
	Clean	Polluted	Clean	Polluted
Cloud droplets	178.9	430.9	11.4	8.0
Rain drops	0.131	0.011	124.2	208.8
Ice crystals	37.5	272.2	30.7	21.9
Snow	1.069	0.381	65.4	60.0
Graupel	0.076	0.015	291.5	422.9
Hail	6.0×10^{-7}	4.6×10^{-7}	2,204	3,311

from the arrangement of an upper-level (8–12 km) negative-charge region and a positive-charge region at lower levels (5–8 km) in the Ctrl and polluted cases (Figure 8). Under these conditions, lightning flashes were initiated between 6 and 10 km (Figure 12b), related to the interface between the upper negative- and lower positive-charge regions. The occurrence of IC flashes illustrates that the lightning channels had sufficient electric potential to penetrate these regions. Basically, the downward vertical channel is followed downward as long as the electric field maintains the same sign. In this study, a CG discharge is identified if the following criteria are satisfied: (a) the channel reaches down to -5°C , (b) there is a correct lower-charge region (e.g., negative charge for +CG and positive charge for -CG), (c) the starting point has an electric potential $>+50 \text{ MV}$ for +CG ($<-50 \text{ MV}$ for -CG), and (d) $|E| > E_{\text{init}} - \delta E_{\text{init}}$ (M01). Only if the difference in the electric potentials of the negative- and positive-charge centers is sufficient to provide a channel with positive potential so that it can propagate to the ground, these charge centers would become the source of +CG flashes. Under polluted conditions, the initiation of +CG flashes indicates that the positive-charge center was the main source of +CG flashes. In the clean run, LCCs were concentrated in the region between about 6 and 12 km (Figure 12a), meaning that the lightning channels between the upper positive- and lower negative-charge centers mainly generated IC flashes. The charge separation in the clean case was insufficient for electric field magnitudes to exceed the breakdown threshold to propagate to the ground. As a result, barely any +CG occurred in the clean case, further indicating that the occurrence of +CG lightning was mainly attributed to the lower positive-charge region (4–6 km) of inverted-polarity charge distribution in the Ctrl and polluted runs. The fraction of +CG lightning was much higher in the polluted run than in the Ctrl run, probably due to the larger ice-phase particle content, higher charging rates, and corresponding greater charge density, as previously discussed.

3.3. Microphysics, Charge Structure, and Lightning Activity

A clear +CG flash occurred at around $t = 145 \text{ min}$ in the polluted case (Figure 11c). To explore the relationships between microphysical and electrical processes, Figure 13 shows vertical cross-sections of different variables from the occurrence of this +CG flash for the polluted case. In the clean case, barely any +CG strokes occurred. Vertical profiles during a similar period are shown in Figure 14 to analyze the effects of aerosols on these processes, which correspond to the occurrence of an earlier -CG event under clean conditions (at $t = 120 \text{ min}$).

There were two major charge regions in the polluted case, namely, an upper negative-charge region (above 6.5 km) and a lower positive-charge region. This positive-charge region mainly arose from graupel particles acquiring positive charges in the presence of larger liquid water contents (Figure 13b; Saunders & Peck, 1998). Charged ice and snow particles led to the negative-charge region in upper levels. An additional negative-charge center appeared at 3–5 km, corresponding to the negatively charged graupel. Stronger updrafts transported more supercooled CWCs to upper levels (above $\sim 4 \text{ km}$), leading to a further increase in ice-phase particles, with 45-dBZ echo tops reaching 12 km (Figure 13c). These increased charged ice-phase particles further led to higher charge densities in the upper levels of the thunderstorm (Figure 13a). By contrast, the simulated charge distribution under clean conditions resulted from snow and ice particles charged positively between 8 and 13 km, and graupel and hail charged negatively between 5 and 8 km (Figures 14b and 14d). The polarities of charged hydrometeors at different levels were mainly due to the different temperatures and supercooled CWC for different CCN concentrations. Concerning the charge density, the peak positive-charge density in the upper levels

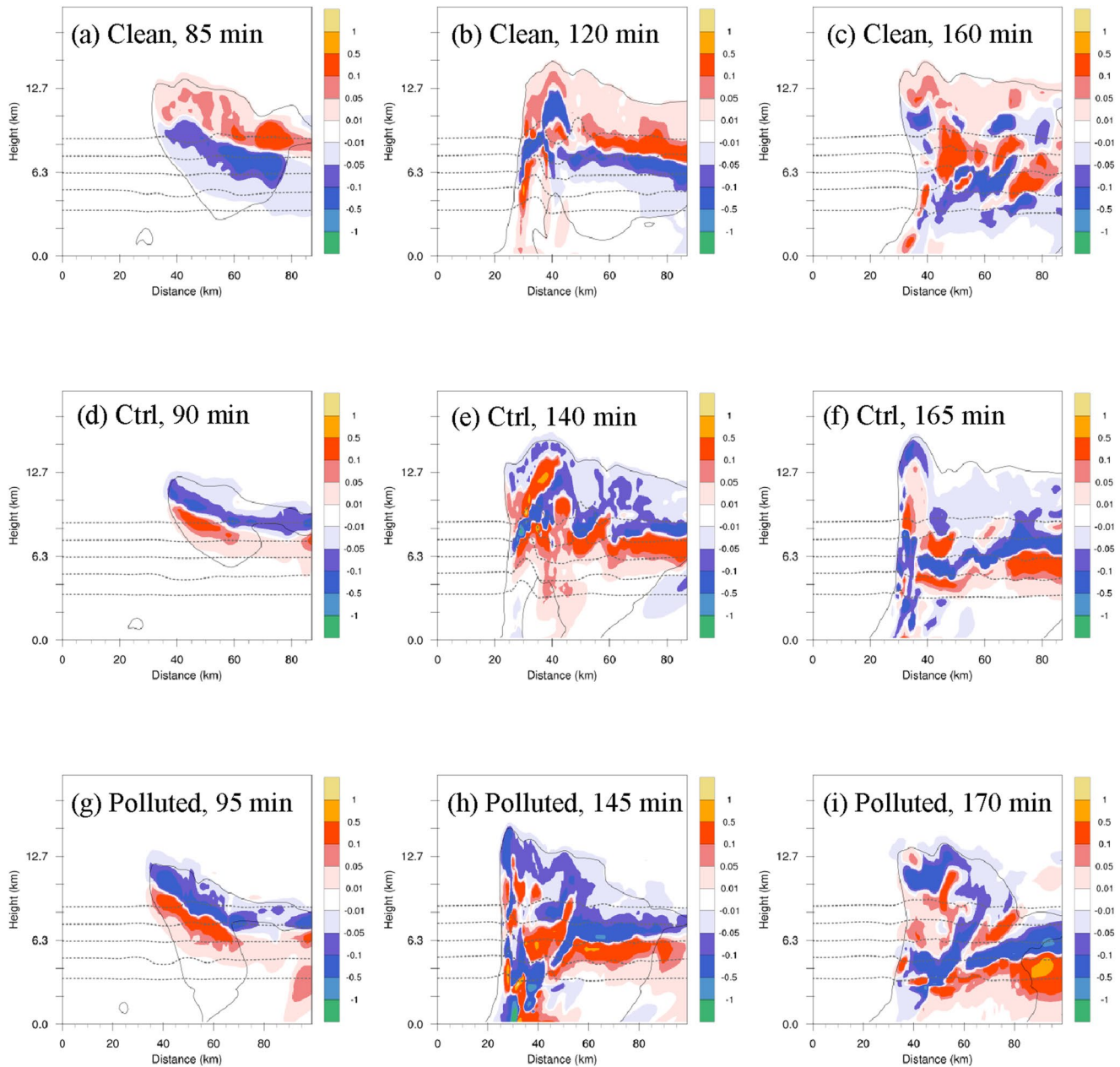


Figure 8. Simulated charge structure (nC m^{-3} , shaded) at the location shown in Figure 2b. (a–c) Clean-case simulations at 85, 120, and 160 min (d–f) Ctrl-case simulations at 90, 140, and 165 min (g–i) Polluted-case simulations at 95, 145, and 170 min. Dashed lines in (a)–(i) show the 0°C , -10°C , -20°C , -30°C , and -40°C isotherms.

in the polluted run reached $+1.0 \text{ nC m}^{-3}$. The maximum of that in the clean case was much less (Figures 13a and 14a). As previously discussed, convection in the polluted run was stronger than in the clean run. Therefore, more ice crystals and graupel particles with larger sizes could be lifted to the upper levels. Collisions of these particles strengthened electrification processes, further contributing to the higher charge density above 10 km (Figure 13a). Under polluted conditions, graupel and other ice-phase particles were mainly charged positively at upper levels ($<-40^\circ\text{C}$) in the presence of stronger updrafts and higher supercooled CWCs. This explains the formation of the stronger positive-charge center at 4–6 km in the core of convection, important for the occurrence of +CG flashes under high CCN concentration conditions.

We attempted to investigate the source of +CG flashes by examining vertical profiles of LCCs at the pre-mature stage for the clean ($t = 120 \text{ min}$) and polluted ($t = 145 \text{ min}$) runs (Figure 15). In the clean case, there were fewer

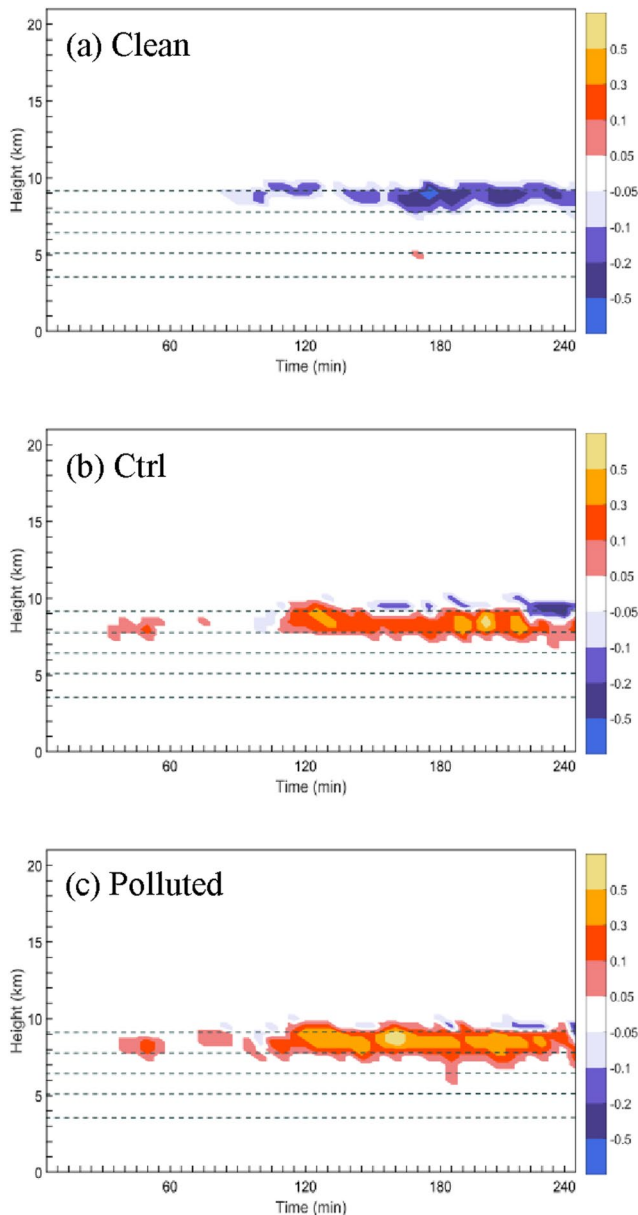


Figure 9. Time-height domain-averaged non-inductive charging rate ($\text{pC m}^{-3} \text{s}^{-1}$, shaded) for the (a) clean, (b) Ctrl, and (c) polluted runs. Dashed contours show the base-state 0°C , -10°C , -20°C , -30°C , and -40°C isotherms.

positive and negative LCCs than in the polluted run. Both positive and negative LCCs in the polluted run were about four times that of the clean run. The “inverted” polarity charge distribution was manifested in the discharge processes, with positive (and negative) channels at $T < -30^\circ\text{C}$, generating IC flashes between the upper charge regions (Figures 13a and 15b). As noted by Mansell et al. (2002), a lower negative-charge region is required for the initiation of simulated +CG flashes like the role of the lower positive-charge for -CG flashes. The main positive-charge center was significant enough to initiate +CG strokes in the presence of a lower negative-charge region at 4–6 km, showing positive channels in the 0°C to -20°C layer between these charge regions (Figure 15b). Figure 15b shows a few negative-channel volumes near the ground. These near-ground channels may have come from IC flashes, which can get fairly low, but the potential surface was likely too large in this situation and maybe unrealistic. In the clean case, it is difficult to reach the breakdown threshold of the electric field due to the much lower charge density (Fierro et al., 2015). Positive and negative lightning channels mainly arose from the charge regions in the upper levels (6–8 km) in this case. Fewer LCCs were produced, with even fewer reaching the ground, which explains the weaker lightning discharge and fewer CG flashes in the clean case.

4. Conclusions and Discussion

To illuminate the aerosol effects on the intensity and polarity of lightning activity, a three-dimensional lightning scheme (MacGorman et al., 2001) was coupled in the WRF model to simulate an idealized supercell thunderstorm. In addition to a baseline run representing a real situation, sensitivity experiments were conducted under clean and polluted conditions by changing the CCN concentration. The similarity of convective and lightning behaviors between observed and simulated (Ctrl run) storms suggests that our idealized simulation provided at least some of the critical storm characteristics in the 2 June 1995 thunderstorms. Our results indicate that lightning flash rates were enhanced by the elevated CCN concentration, accompanied by a significantly increased percentage of +CG flashes in the polluted case. Figure 16 illustrates these gained insights.

Differences in lightning activity between different aerosol scenarios mainly resulted from microphysical processes. Increased CCN concentrations increased the number of cloud droplets and ice-phase particles. The formation of more cloud water strengthened the convection under polluted conditions, with stronger updrafts at upper levels and a larger 55-dBZ echo volume. Smaller droplets suppressed the collection-coalescence process, leading to less rain water under polluted conditions. These droplets not accreted by raindrops were lifted to higher levels. This enhanced mixed-phase processes, with more ice-phase particles generated at upper levels, mainly resulting

from the homogeneous freezing of smaller cloud droplets. The release of latent heat associated with freezing further invigorated convection in the polluted case. The graupel and snow particle contents were less under polluted conditions due to the smaller rain water content and thus less effective collection of raindrops by graupel and snow particles. However, the sizable amount of ice crystals and larger graupel (and hail) particles in the upper levels ensured sufficient charge separation in the presence of supercooled liquid water under polluted conditions.

As indicated by the non-inductive charging mechanism (Saunders & Peck, 1998), graupel particles are mainly charged positively at upper levels, where there are stronger updrafts and higher CWCs. Here, the gross charge distribution resembled an “inverted” polarity charge structure under polluted conditions, with negative charge above the main positive-charge region. Electrification was evidently strengthened due to sufficient collisions between larger graupel (and hail) and other ice-phase particles, leading to a higher charge density in the

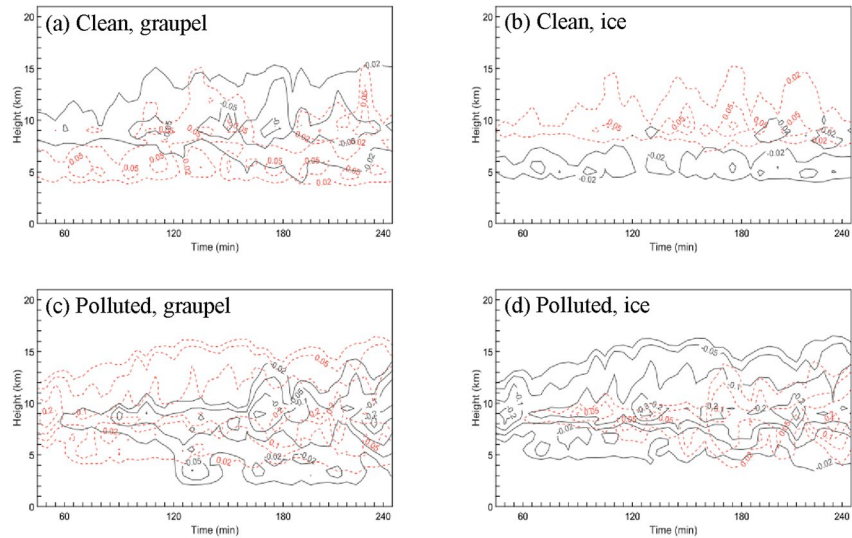


Figure 10. Temporal variations of peak values of positive (red dashed lines) and negative (solid lines) charge density (unit: nC m^{-3}) carried by (a), (c) graupel particles and (b), (d) ice crystals for the (top) clean and (bottom) polluted runs. Contours for positive (or negative) charge density are ± 0.02 , ± 0.05 , ± 0.1 , ± 0.2 , and $\pm 0.3 \text{ nC m}^{-3}$.

polluted case. As a result, positively charged ice-phase hydrometeors led to a stronger positive-charge region at lower levels. Lightning discharges occur only if the charge density is sufficient for electric field magnitudes to exceed the breakdown value. The higher charge density partly explains the enhanced lightning activity (IC and CG flashes) owing to the elevated CCN concentration. This main positive-charge center is significant for the occurrence of IC and +CG flashes. Under polluted conditions, positive channels originating from the main positive-charge region can propagate to the ground due to the higher charge density, forming +CG flashes. Therefore, total lightning flashes increased with the added CCN concentration, as did the percentage of +CG strokes. The lower negative-charge region under the main positive-charge center was also important for the initiation of +CG flashes in the polluted case, noted by Mansell et al. (2002). Under clean conditions, lower charge density resulted in fewer lightning discharges. The normal polarity charge structure, with mid-level negative charge below the positive charge, mainly generated IC flashes between these charge regions. The main positive-charge region of the inverted charge structure in the polluted case played a critical role in the initiation of +CG flashes. Even if there were CG flashes in the clean case, it would be difficult to initiate +CG flashes without the existence of a mid-level positive-charge region.

Results reported here support the aerosol hypothesis for charge separation and lightning production. We found that total lightning, particularly the percentage of +CG lightning flashes, increased under polluted conditions, consistent with observations (e.g., Liu et al., 2021; Naccarato et al., 2003). However, aerosols have complicated influences on ice production and updrafts, meaning that the relationship between aerosols and lightning is likely non-monotonic. Too many aerosols may inhibit convection or ice production and reduce the number of lightning flashes (e.g., Altaratz et al., 2010; Hu et al., 2019; Mansell & Ziegler, 2013). In this study, we also found a higher percentage of +CG strokes in the polluted case, originating from lower positive-charge regions with stronger

Table 2
Charge Densities of Ice-Phase Particles

	Average ($10^{-5} \text{ nC m}^{-3}$)		Maximum positive (nC m^{-3})		Maximum negative (nC m^{-3})	
	Clean	Polluted	Clean	Polluted	Clean	Polluted
Ice crystals	+1.16	-1.84	0.136	0.310	-0.071	-0.387
Graupel	-1.18	+1.61	0.083	0.301	-0.160	-0.342
Snow	+1.04	-0.33	0.669	1.179	-0.747	-1.228
Hail	0.00	+0.30	0.043	0.335	-0.035	-0.084

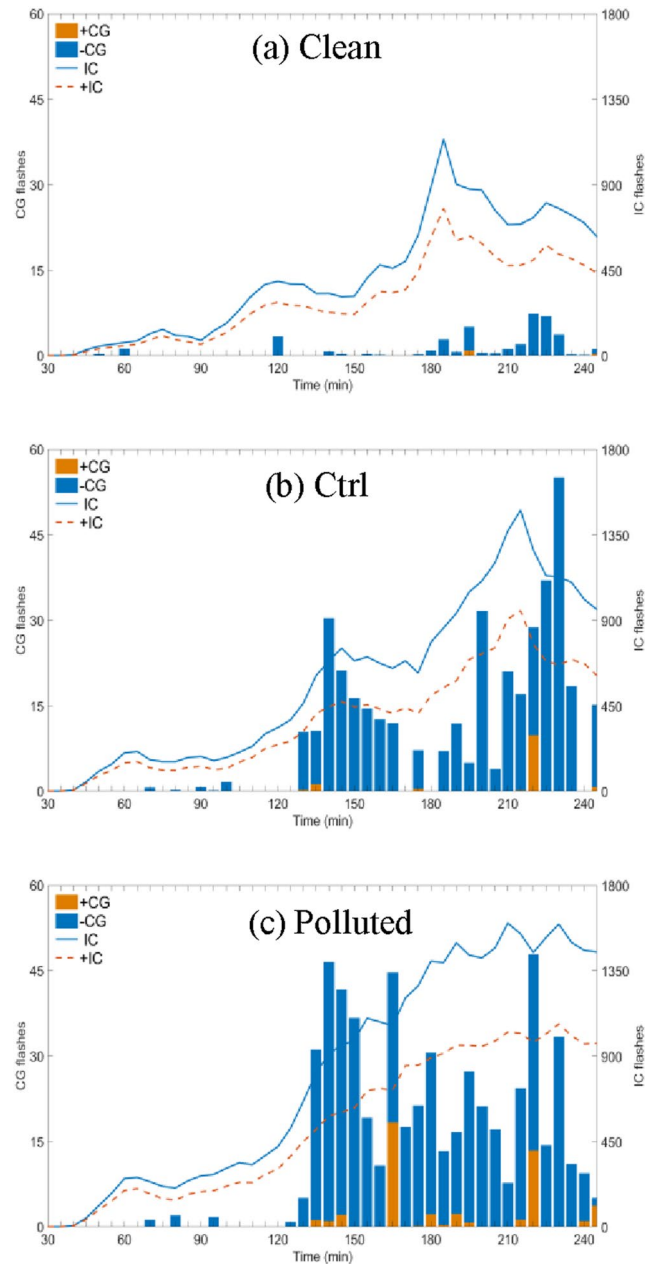


Figure 11. Temporal variations of simulated lightning frequency (unit: $\text{fl } 5 \text{ min}^{-1}$) for the (a) clean, (b) Ctrl, and (c) polluted runs. Solid lines represent total intra-cloud (IC) flashes, and dashed lines represent +IC flashes. Orange bars represent +CG flashes, and blue bars represent -CG flashes. Dashed gray lines show the base-state 0°C , -10°C , -20°C , -30°C , and -40°C isotherms.

charge densities. Positive lightning channels from this region could propagate to the ground, forming more +CG strokes. There were very few +CG strokes in the clean case. Previous observational studies have reported the enhancement of +CG flashes in polluted scenarios, speculating that it was due to the charge configuration with an enhanced lower positive-charge region (e.g., Yair et al., 2021). Less obvious aerosol effects on simulated storm charge structure polarity were reported by Mansell and Ziegler (2013). More observational and simulation studies are thus needed to further investigate the effect of aerosols on lightning intensity and polarity.

This study simulated a supercell thunderstorm that occurred in western Texas, but whether our findings are also seen in other types of storms or other regions of the world is unknown. Analyzing different types of storms, which can be created by adjusting the environment in idealized configurations (e.g., Storer et al., 2010; Sun,

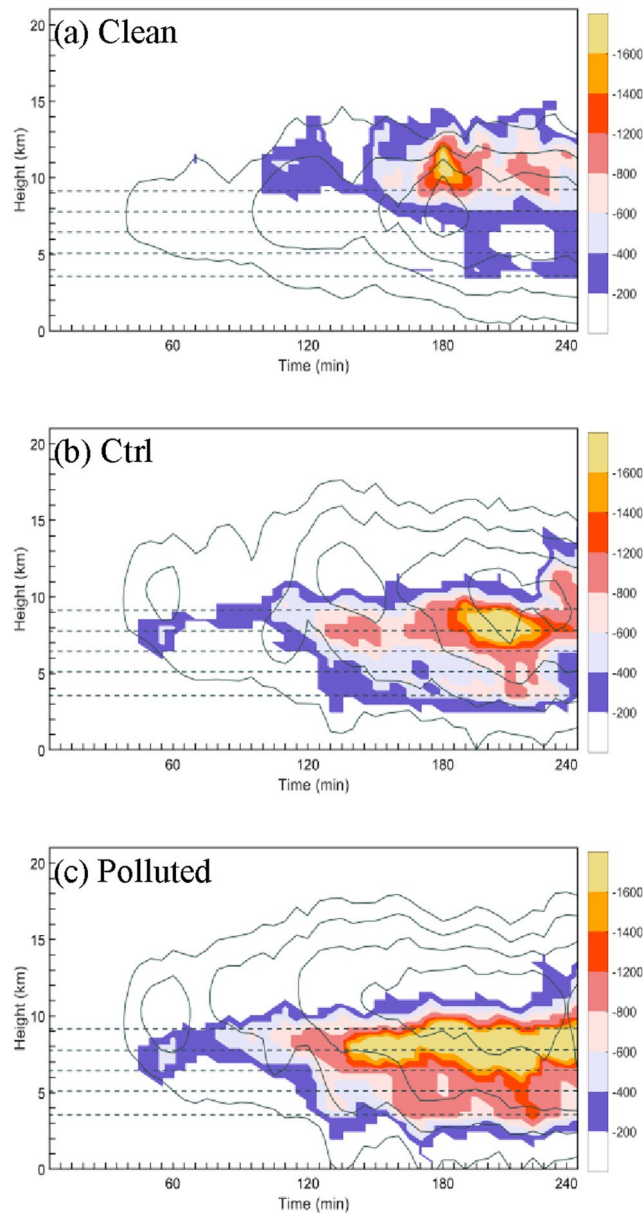


Figure 12. Time-height variations of horizontally domain-averaged positive (solid line, unit: 5 min^{-1}) and negative (shaded, unit: 5 min^{-1}) lightning channel counts (LCCs) for the (a) clean, (b) Ctrl, and (c) polluted runs. Contours for positive LCCs are 50, 200, 500, and 1,000 (5 min^{-1}). Dashed gray lines show the base-state 0°C , -10°C , -20°C , -30°C , and -40°C isotherms.

Qie, et al., 2023), may be warranted. Furthermore, an inverted cloud polarity has often been found in the region of specific thermodynamical conditions (Williams et al., 2005). The roles of aerosol and thermodynamics (e.g., cloud base height, dry bulb temperature) are strongly needed to distinguish, based on collaborative observations in both aspects. Note that the current parameterization in the simulations does not use droplet size to determine non-inductive charging. Some studies have found that large droplets lead to more negatively charged graupel (Avila & Pereyra, 2000). On the contrary, Takahashi (1978) suggested that the impact of droplet size on non-inductive charging was negligible. This presents a challenge for the parameterization of electrification in lightning models. It may be that the varied droplet-size dependence of non-inductive charging could influence the aerosol effects on charge separation and associated lightning polarity.

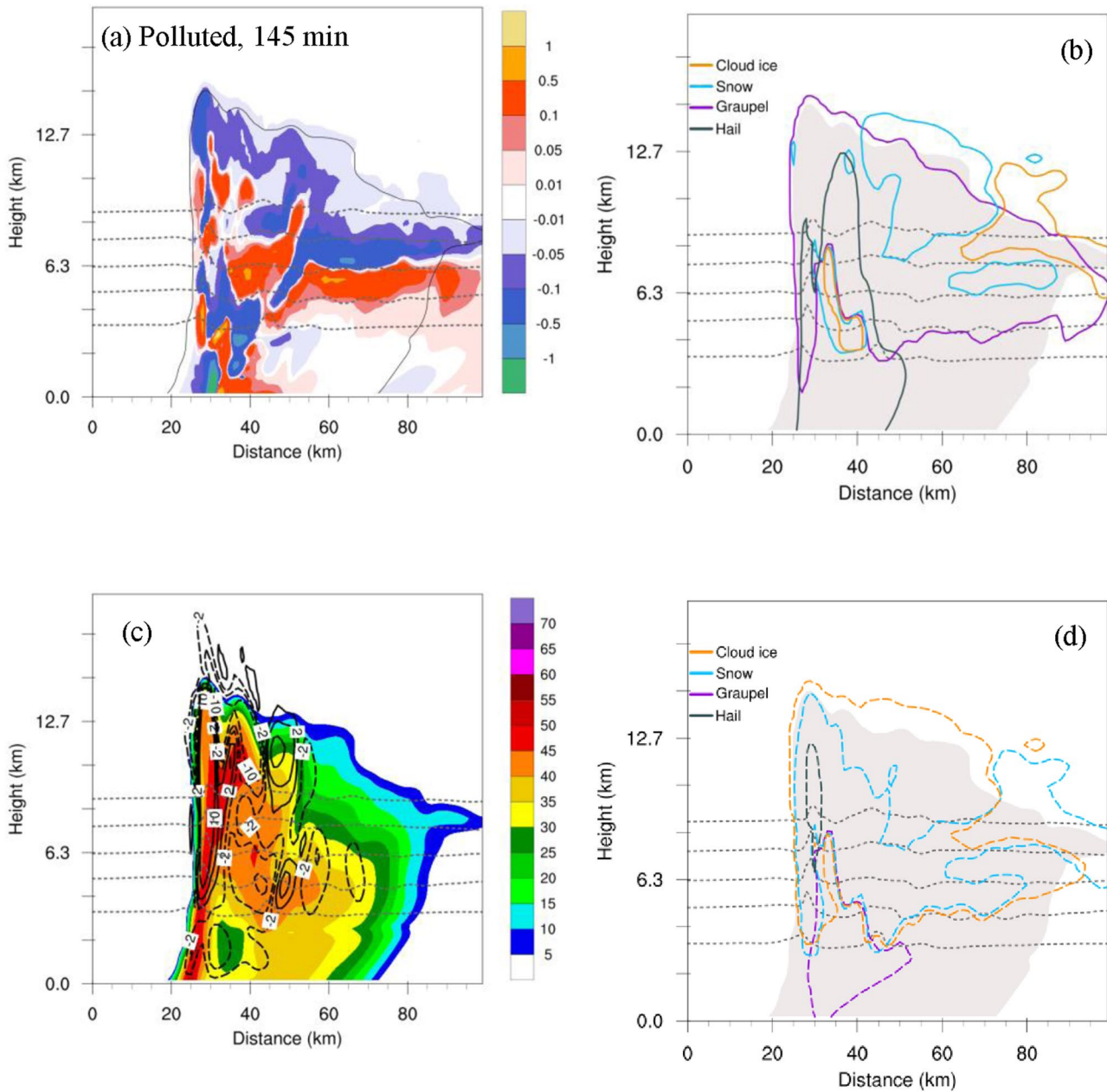


Figure 13. Vertical sections (west to east) at the location illustrated in Figure 2h at the pre-mature stage of the thunderstorm (145 min) in the polluted run. (a) Charge structure (nC m^{-3} , shaded). (b) $+0.1 \text{ nC m}^{-3}$ charge density contours for ice (orange), graupel (purple), snow (blue), and hail (black). (c) Radar reflectivity (dBZ), where black lines show vertical velocities (solid line: 2, 5, 10 m s^{-1} ; dashed line: -2, -5, -10 m s^{-1}). (d) As in (b), but for the -0.1 nC m^{-3} charge density. The cloud outline (reflectivity echoes $\geq 5 \text{ dBZ}$) is denoted by the gray shaded areas in (b) and (d). Dashed gray lines show the base-state 0°C , -10°C , -20°C , -30°C , and -40°C isotherms.

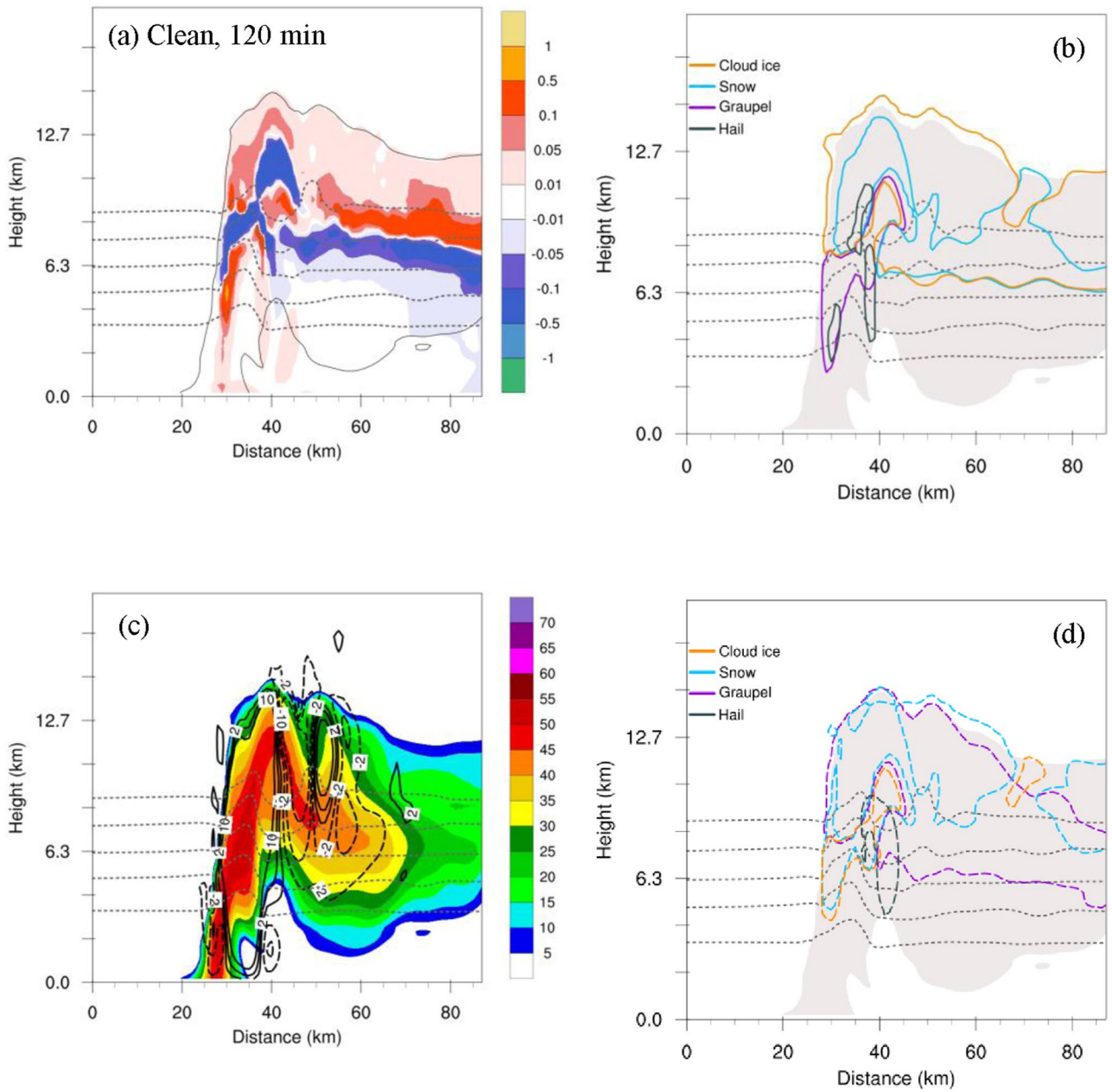


Figure 14. As in Figure 13, but for simulated variables at the pre-mature stage (120 min) in the clean run.

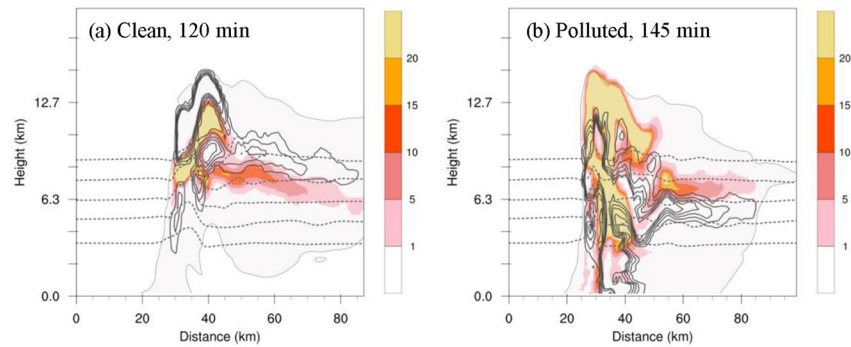


Figure 15. Vertical cross-sections (north to south) at the locations shown in Figure 2 of positive (shaded) and negative (solid line: -1 , -5 , -10 , -15 , -20) lightning channel counts at the pre-mature stage of the (a) clean run (120 min, Figure 2b) and (b) polluted run (145 min, Figure 2h). Dashed gray lines show the base-state 0°C , -10°C , -20°C , -30°C , and -40°C isotherms.

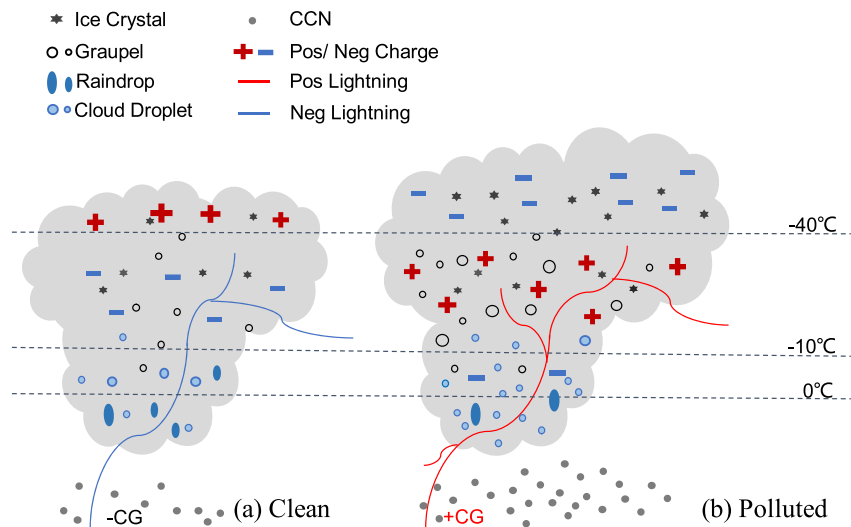


Figure 16. Schematic illustration of the aerosol effects on electrification and lightning polarity. In the clean atmosphere (left), there are lower charge density and fewer lightning discharges as a result of less ice-phase particle content. Negatively charged graupel particles at lower supercooled cloud water content (CWC) form a dipole charge structure, leading to discharges dominated by negative polarity. Added aerosols (right) increase the cloud droplet number that can be lifted above the freezing level, leading to higher supercooled CWC. The increased ice particle content and graupel size enhance charge separation, yielding more lightning discharges. Positively charged graupel particles at higher supercooled CWC generate a strong positive-charge region in the middle level, so an inverted-polarity charge structure appears. Lightning channels originating from this positive-charge region propagate to the ground, producing more +CG strokes. Note that the positive (and negative) lightning shown in the figure is mainly to distinguish the differences between the clean and polluted conditions and does not represent all types of lightning.

Data Availability Statement

The WRF-ELEC model (version 4.3.1; Skamarock et al., 2008) and corresponding modifications to the code and sophisticated lightning schemes (MacGorman et al., 2001; Mansell et al., 2005) were used for simulating the idealized supercell thunderstorm, available at <https://github.com/MicroTed/WRFV4/tree/release-v4.3.1-elec/>. The input data used for the simulations is available in the Zenodo repository (Sun, Li, et al., 2023).

Acknowledgments

This research was supported by the National Natural Science Foundation of China (42030606) and the Hong Kong Polytechnic University (PolyU) Postdoctoral Fellowship.

References

Altaratz, O., Koren, I., Yair, Y., & Price, C. (2010). Lightning response to smoke from Amazonian fires. *Geophysical Research Letters*, *37*(7), L07801. <https://doi.org/10.1029/2010GL042679>

Avila, E. A., & Pereyra, R. G. (2000). Charge transfer during crystal-graupel collisions for two different cloud droplet size distributions. *Geophysical Research Letters*, *27*(23), 3837–3840. <https://doi.org/10.1029/2000GL012302>

Bell, T. L., Rosenfeld, D., & Kim, K.-M. (2009). Weekly cycle of lightning: Evidence of storm invigoration by pollution. *Geophysical Research Letters*, *36*(23), L23805. <https://doi.org/10.1029/2009GL040915>

Carey, L. D., Rutledge, S. A., & Petersen, W. A. (2003). The relationship between severe storm reports and cloud-to-ground lightning polarity in the contiguous United States from 1989 to 1998. *Monthly Weather Review*, *131*(7), 1211–1228. [https://doi.org/10.1175/1520-0493\(2003\)131<1211:TRBSSR>2.0.CO;2](https://doi.org/10.1175/1520-0493(2003)131<1211:TRBSSR>2.0.CO;2)

Coquillat, S., Boussaton, M.-P., Buguet, M., Lambert, D., Ribaud, J.-F., & Berthelot, A. (2013). Lightning ground flash patterns over Paris area between 1992 and 2003: Influence of pollution? *Atmospheric Research*, *122*, 77–92. <https://doi.org/10.1016/j.atmosres.2012.10.032>

Dendy, J. E., Jr., & Moulton, J. D. (2010). Black box multigrid with coarsening by a factor of three. *Numerical Linear Algebra with Applications*, *17*, 577–598. <https://doi.org/10.1002/nla.705>

Dwyer, J. R. (2003). A fundamental limit on electric fields in air. *Geophysical Research Letters*, *30*(20), 2055. <https://doi.org/10.1029/2003GL017781>

Dye, J. E., Knight, C. A., Toutenhoofd, V., & Cannon, T. W. (1974). The mechanism of precipitation formation in northeastern Colorado Cumulus III. Coordinated microphysical and radar observations and summary. *Journal of the Atmospheric Sciences*, *31*(8), 2152–2159. [https://doi.org/10.1175/1520-0469\(1974\)031<2152:TMOPFI>2.0.CO;2](https://doi.org/10.1175/1520-0469(1974)031<2152:TMOPFI>2.0.CO;2)

Fan, J., Leung, L. R., Rosenfeld, D., & DeMott, P. J. (2017). Effects of cloud condensation nuclei and ice nucleating particles on precipitation processes and supercooled liquid in mixed-phase orographic clouds. *Atmospheric Chemistry and Physics*, *17*(2), 1017–1035. <https://doi.org/10.5194/acp-17-1017-2017>

Fernandes, W. A., Pinto, I. R. C. A., Pinto, O., Longo, K. M., & Freitas, S. R. (2006). New findings about the influence of smoke from fires on the cloud-to-ground lightning characteristics in the Amazon region. *Geophysical Research Letters*, *33*(20), L20810. <https://doi.org/10.1029/2006GL027744>

Feudale, L., & Manzato, A. (2014). Cloud-to-ground lightning distribution and its relationship with orography and anthropogenic emissions in the Po Valley. *Journal of Applied Meteorology and Climatology*, *53*(12), 2651–2670. <https://doi.org/10.1175/jamc-d-14-0037.1>

Fierro, A. O., Gilmore, M. S., Mansell, E. R., Wicker, L. J., & Straka, J. M. (2006). Electrification and lightning in an idealized boundary-crossing supercell simulation of 2 June 1995. *Monthly Weather Review*, *134*(11), 3149–3172. <https://doi.org/10.1175/MWR3231.1>

Fierro, A. O., Mansell, E. R., MacGorman, D. R., & Ziegler, C. L. (2013). The implementation of an explicit charging and discharge lightning scheme within the WRF-ARW model: Benchmark simulations of a continental squall line, a tropical cyclone, and a winter storm. *Monthly Weather Review*, *141*(7), 2390–2415. <https://doi.org/10.1175/MWR-D-12-00278.1>

Fierro, A. O., Mansell, E. R., Ziegler, C. L., & MacGorman, D. R. (2015). Explicitly simulated electrification and lightning within a tropical cyclone based on the environment of Hurricane Isaac (2012). *Journal of the Atmospheric Sciences*, *72*(11), 4167–4193. <https://doi.org/10.1175/JAS-D-14-0374.1>

Gilmore, M. S. (2000). Observed and simulated 2–3 June 1995 west Texas Panhandle supercells Ph.D. dissertation (p. 250). Texas A&M. [Available from Evans Library, Texas A&M University, College Station, TX 77843.]

Gilmore, M. S., & Wicker, L. J. (2002). Influences of the local environment on supercell cloud-to-ground lightning, radar characteristics, and severe weather on 2 June 1995. *Monthly Weather Review*, *130*(10), 2349–2372. [https://doi.org/10.1175/1520-0493\(2002\)130<2349:IOTLEO>2.0.CO;2](https://doi.org/10.1175/1520-0493(2002)130<2349:IOTLEO>2.0.CO;2)

Guo, J., Deng, M., Lee, S. S., Wang, F., Li, Z., Zhai, P., et al. (2016). Delaying precipitation and lightning by air pollution over the Pearl River Delta. Part I: Observational analyses. *Journal of Geophysical Research: Atmospheres*, *121*(11), 6472–6488. <https://doi.org/10.1002/2015JD023257>

Hu, J. X., Rosenfeld, D., Ryzhkov, A., Zrnic, D., Williams, E., Zhang, P. F., et al. (2019). Polarimetric radar convective cell tracking reveals large sensitivity of cloud precipitation and electrification properties to CCN. *Journal of Geophysical Research: Atmospheres*, *124*(22), 12194–12205. <https://doi.org/10.1029/2019jd030857>

Khain, A., Lynn, B., & Dudhia, J. (2010). Aerosol effects on intensity of landfalling hurricanes as seen from simulations with the WRF model with spectral bin microphysics. *Journal of the Atmospheric Sciences*, *67*(2), 365–384. <https://doi.org/10.1175/2009JAS3210.1>

Kuhlman, K. M., Ziegler, C. L., Mansell, E. R., MacGorman, D. R., & Straka, J. M. (2006). Numerically simulated electrification and lightning of the 29 June 2000 STEPS supercell storm. *Monthly Weather Review*, *134*(10), 2734–2757. <https://doi.org/10.1175/MWR3217.1>

Li, Z., Lau, W. K.-M., Ramanathan, V., Wu, G., Ding, Y., Manoj, M. G., et al. (2016). Aerosol and monsoon interactions in Asia. *Reviews of Geophysics*, *54*(4), 866–929. <https://doi.org/10.1002/2015RG000500>

Li, Z., Wang, Y., Guo, J. P., Zhao, C. F., Cribb, M. C., Dong, X. Q., et al. (2019). East Asian study of tropospheric aerosols and their impact on regional clouds, precipitation, and climate (EAST-AIR_{PC}). *Journal of Geophysical Research: Atmospheres*, *124*(23), 13026–13054. <https://doi.org/10.1029/2019jd030758>

Liu, Y., Williams, E., Li, Z., Guha, A., Lapierre, J., Stock, M., et al. (2021). Lightning enhancement in moist convection with smoke-laden air advected from Australian wildfires. *Geophysical Research Letters*, *48*(11), e2020GL092355. <https://doi.org/10.1029/2020GL092355>

Lu, J., Qie, X., Xiao, X., Jiang, R., Mansell, E. R., Fierro, A. O., et al. (2022). Effects of convective mergers on the evolution of microphysical and electrical activity in a severe squall line simulated by WRF coupled with explicit electrification scheme. *Journal of Geophysical Research: Atmospheres*, *127*(16), e2021JD036398. <https://doi.org/10.1029/2021JD036398>

Lynn, B. H., Khain, A., Rosenfeld, D., & Woodley, W. L. (2007). Effects of aerosols on precipitation from orographic clouds. *Journal of Geophysical Research*, *112*(D10), D10225. <https://doi.org/10.1029/2006JD007537>

Lyons, W. A., Nelson, T. E., Williams, E. R., Cramer, J. A., & Turner, T. R. (1998). Enhanced positive cloud-to-ground lightning in thunderstorms ingesting smoke from fires. *Science*, *282*(5386), 77–80. <https://doi.org/10.1126/science.282.5386.77>

MacGorman, D. R., Straka, J. M., & Ziegler, C. L. (2001). A lightning parameterization for numerical cloud models. *Journal of Applied Meteorology and Climatology*, *40*(3), 459–478. [https://doi.org/10.1175/1520-0450\(2001\)040<0459:ALPENC>2.0.CO;2](https://doi.org/10.1175/1520-0450(2001)040<0459:ALPENC>2.0.CO;2)

Mansell, E. R., MacGorman, D. R., Ziegler, C. L., & Straka, J. M. (2002). Simulated three-dimensional branched lightning in a numerical thunderstorm model. *Journal of Geophysical Research*, *107*(D9), 4075. <https://doi.org/10.1029/2000JD000244>

Mansell, E. R., MacGorman, D. R., Ziegler, C. L., & Straka, J. M. (2005). Charge structure and lightning sensitivity in a simulated multicell thunderstorm. *Journal of Geophysical Research*, *110*(D12), D12101. <https://doi.org/10.1029/2004JD005287>

Mansell, E. R., & Ziegler, C. L. (2013). Aerosol effects on simulated storm electrification and precipitation in a two-moment bulk microphysics model. *Journal of the Atmospheric Sciences*, *70*(7), 2032–2050. <https://doi.org/10.1175/JAS-D-12-0264.1>

Mansell, E. R., Ziegler, C. L., & Bruning, E. C. (2010). Simulated electrification of a small thunderstorm with two-moment bulk microphysics. *Journal of the Atmospheric Sciences*, *67*(1), 171–194. <https://doi.org/10.1175/2009jas2965.1>

- Mitzeva, R., Latham, J., & Petrova, S. (2006). A comparative modeling study of the early electrical development of maritime and continental thunderstorms. *Atmospheric Research*, 82(1–2), 26–36. <https://doi.org/10.1016/j.atmosres.2005.01.006>
- Murray, N. D., Orville, R. E., & Huffines, G. R. (2000). Effect of pollution from Central American fires on cloud-to-ground lightning in May 1998. *Geophysical Research Letters*, 27(15), 2249–2252. <https://doi.org/10.1029/2000gl011656>
- Naccarato, K. P., Pinto, O., & Pinto, I. R. C. A. (2003). Evidence of thermal and aerosol effects on the cloud-to-ground lightning density and polarity over large urban areas of Southeastern Brazil. *Geophysical Research Letters*, 30(13), 1674. <https://doi.org/10.1029/2003GL017496>
- Orville, R. E., Huffines, G. R., Nielsen-Gammon, J., Zhang, R., Ely, B., Steiger, S., et al. (2001). Enhancement of cloud-to-ground lightning over Houston, Texas. *Geophysical Research Letters*, 28(13), 2597–2600. <https://doi.org/10.1029/2001gl012990>
- Qie, K., Qie, X., & Tian, W. (2021). Increasing trend of lightning activity in the South Asia region. *Science Bulletin*, 66(1), 78–84. <https://doi.org/10.1016/j.scib.2020.08.033>
- Qie, X., Zhang, T., Chen, C., Zhang, G., Zhang, T., & Wei, W. (2005). The lower positive charge center and its effect on lightning discharges on the Tibetan Plateau. *Geophysical Research Letters*, 32(5), L05814. <https://doi.org/10.1029/2004GL022162>
- Rosenfeld, D., Lohmann, U., Raga, G. B., O'Dowd, C. D., Kulmala, M., Fuzzi, S., et al. (2008). Flood or drought: How do aerosols affect precipitation? *Science*, 321(5894), 1309–1313. <https://doi.org/10.1126/science.1160606>
- Saunders, C. P. R., & Peck, S. L. (1998). Laboratory studies of the influence of the rime accretion rate on charge transfer during crystal/graupel collisions. *Journal of Geophysical Research*, 103(D12), 13949–13956. <https://doi.org/10.1029/97JD02644>
- Schultz, C. J., Petersen, W. A., & Carey, L. D. (2011). Lightning and severe weather: A comparison between total and cloud-to-ground lightning trends. *Weather and Forecasting*, 26(5), 744–755. <https://doi.org/10.1175/WAF-D-10-05026.1>
- Shi, Z., Tan, Y., Tang, H., & Coauthors (2015). A numerical study of aerosol effects on the electrification and flash rate of thunderstorms. *Chinese Journal of Atmospheric Sciences*, 39, 941–952. (in Chinese). <https://doi.org/10.3878/j.issn.1006-9895.1412.14230>
- Skamarock, W. C., Klemp, J. B., Dudhia, J., Gill, D. O., Barker, D., Duda, M. G., et al. (2008). *A description of the advanced research WRF version 3 (No. NCAR/TN-475+STR)*. University Corporation for Atmospheric Research. <https://doi.org/10.5065/D68S4MVH>
- Stallins, J. A., Carpenter, J., Bentley, M. L., Ashley, W. S., & Mulholland, J. A. (2013). Weekend–weekday aerosols and geographic variability in cloud-to-ground lightning for the urban region of Atlanta, Georgia, USA, Reg. *Environment & Change*, 13(1), 137–151. <https://doi.org/10.1007/s10113-012-0327-0>
- Storer, R. L., van den Heever, S. C., & Stephens, G. L. (2010). Modeling aerosol impacts on convective storms in different environments. *Journal of the Atmospheric Sciences*, 67(12), 3904–3915. <https://doi.org/10.1175/2010JAS3363.1>
- Straka, J. M., & Mansell, E. R. (2005). A bulk microphysics parameterization with multiple ice precipitating categories. *Journal of Applied Meteorology*, 44(4), 445–466. <https://doi.org/10.1175/JAM2211.1>
- Sun, M., Li, Z., Wang, T., Mansell, E. R., Qie, X., Shan, S., et al. (2023). Understanding the effects of aerosols on electrification and lightning polarity in an idealized supercell thunderstorm via model emulation [Dataset]. Zenodo. <https://doi.org/10.5281/zenodo.8372378>
- Sun, M., Liu, D., Qie, X., Mansell, E. R., Yair, Y., Fierro, A. O., et al. (2021). Aerosol effects on electrification and lightning discharges in a multi-cell thunderstorm simulated by the WRF-ELEC model. *Atmospheric Chemistry and Physics*, 21(18), 14141–14158. <https://doi.org/10.5194/acp-21-14141-2021>
- Sun, M., Qie, X., Mansell, E. R., Liu, D., Yair, Y., Fierro, A. O., et al. (2023). Aerosol impacts on storm electrification and lightning discharges under different thermodynamic environments. *Journal of Geophysical Research: Atmospheres*, 128(8), e2022JD037450. <https://doi.org/10.1029/2022JD037450>
- Takahashi, T. (1978). Riming electrification as a charge generation mechanism in thunderstorms. *Journal of the Atmospheric Sciences*, 35(8), 1536–1548. [https://doi.org/10.1175/1520-0469\(1978\)035<1536:REACG>2.0.CO;2](https://doi.org/10.1175/1520-0469(1978)035<1536:REACG>2.0.CO;2)
- Tan, Y., Ma, X., Xiang, C., & Coauthors (2017). A numerical study of the effects of aerosol on electrification and lightning discharges during thunderstorms. *Chinese Journal of Geophysics*, 60, 3041–3050. (in Chinese). <https://doi.org/10.6038/cjg20170812>
- Thornton, J. A., Virts, K. S., Holzworth, R. H., & Mitchell, T. P. (2017). Lightning enhancement over major oceanic shipping lanes. *Geophysical Research Letters*, 44(17), 9102–9111. <https://doi.org/10.1002/2017GL074982>
- Twomey, S. (1959). The nuclei of natural cloud formation. Part II: The supersaturation in natural clouds and the variation of cloud droplet concentration. *Geofisica Pura e Applicata*, 43(1), 243–249. <https://doi.org/10.1007/BF01993560>
- Van Den Broeke, M. S., Straka, J. M., & Rasmussen, E. N. (2008). Polarimetric radar observations at low levels during tornado life cycles in a small sample of classic Southern Plains supercells. *Journal of Applied Meteorology and Climatology*, 47(4), 1232–1247. <https://doi.org/10.1175/2007JAMC1714.1>
- Wang, Q., Li, Z., Guo, J., Zhao, C., & Cribb, M. (2018). The climate impact of aerosols on the lightning flash rate: Is it detectable from long-term measurements? *Atmospheric Chemistry and Physics*, 18(17), 12797–12816. <https://doi.org/10.5194/acp-18-12797-2018>
- Wang, Y., Wan, Q., Meng, W., Liao, F., Tan, H., & Zhang, R. (2011). Long-term impacts of aerosols on precipitation and lightning over the Pearl River Delta megacity area in China. *Atmospheric Chemistry and Physics*, 11(23), 12421–12436. <https://doi.org/10.5194/acp-11-12421-2011>
- Westcott, N. E. (1995). Summertime cloud-to-ground lightning activity around major Midwestern urban areas. *Journal of Applied Meteorology*, 34(7), 1633–1642. <https://doi.org/10.1175/1520-0450-34.7.1633>
- Williams, E., Mushtak, V., Rosenfeld, D., Goodman, S., & Boccippio, D. (2005). Thermodynamic conditions favorable to superlative thunderstorm updraft, mixed phase microphysics and lightning flash rate. *Atmospheric Research*, 76(1–4), 288–306. <https://doi.org/10.1016/j.atmosres.2004.11.009>
- Yair, Y., Lynn, B., Yaffe, M., Ziv, B., & Shpund, J. (2021). Observations and numerical simulations of the October 25th, 2015 super-cell thunderstorm over central Israel. *Atmospheric Research*, 247, 105165. <https://doi.org/10.1016/j.atmosres.2020.105165>
- Yang, X., Li, X., Liu, L., Zhou, L., Cribb, M., & Zhang, F. (2016). Distinct weekly cycles of thunderstorms and a potential connection with aerosol type in China. *Geophysical Research Letters*, 43(16), 8760–8768. <https://doi.org/10.1002/2016GL070375>
- Yuan, S., Qie, X., Jiang, R., Wang, D., Sun, Z., Srivastava, A., & Williams, E. (2020). Origin of an uncommon multiple-stroke positive cloud-to-ground lightning flash with different terminations. *Journal of Geophysical Research: Atmospheres*, 125(15), e2019JD032098. <https://doi.org/10.1029/2019JD032098>
- Zhao, C., Zhang, Y., Zheng, D., Liu, X., Zhang, Y., Fan, X., et al. (2022). Using polarimetric radar observations to characterize first echoes of thunderstorms and non-thunderstorms: A comparative study. *Journal of Geophysical Research: Atmospheres*, 127(23), e2022JD036671. <https://doi.org/10.1029/2022JD036671>
- Zhao, P., Li, Z., Xiao, H., Wu, F., Zheng, Y., Cribb, M. C., et al. (2020). Distinct aerosol effects on cloud-to-ground lightning in the plateau and basin regions of Sichuan, Southwest China. *Atmospheric Chemistry and Physics*, 20(21), 13379–13397. <https://doi.org/10.5194/acp-20-13379-2020>
- Zhao, P., Yin, Y., & Xiao, H. (2015). The effects of aerosol on development of thunderstorm electrification: A numerical study. *Atmospheric Research*, 153, 376–391. <https://doi.org/10.1016/j.atmosres.2014.09.011>

- Ziegler, C. L., & MacGorman, D. R. (1994). Observed lightning morphology relative to modeled space charge and electric field distributions in a tornadic storm. *Journal of the Atmospheric Sciences*, *51*(6), 833–851. [https://doi.org/10.1175/1520-0469\(1994\)051<0833:OLMRTM>2.0.CO;2](https://doi.org/10.1175/1520-0469(1994)051<0833:OLMRTM>2.0.CO;2)
- Zrnic, D. S., Balakrishnan, N., Ziegler, C. L., Bringi, V. N., Aydin, K., & Matejka, T. (1993). Polarimetric signatures in the stratiform region of a mesoscale convective system. *Journal of Applied Meteorology and Climatology*, *32*(4), 678–693. [https://doi.org/10.1175/1520-0450\(1993\)032<0678:PSITSR>2.0.CO;2](https://doi.org/10.1175/1520-0450(1993)032<0678:PSITSR>2.0.CO;2)